CURBIO, Volume *26*

Supplemental Information

Pleistocene Mitochondrial Genomes Suggest a Single Major Dispersal of Non-Africans and a Late Glacial Population Turnover in Europe

Cosimo Posth, Gabriel Renaud, Alissa Mittnik, Dorothée G. Drucker, Hélène Rougier, Christophe Cupillard, Frédérique Valentin, Corinne Thevenet, Anja Furtwängler, Christoph Wißing, Michael Francken, Maria Malina, Michael Bolus, Martina Lari, Elena Gigli, Giulia Capecchi, Isabelle Crevecoeur, Cédric Beauval, Damien Flas, Mietje Germonpré, Johannes van der Plicht, Richard Cottiaux, Bernard Gély, Annamaria Ronchitelli, Kurt Wehrberger, Dan Grigorescu, Jiří Svoboda, Patrick Semal, David Caramelli, Hervé Bocherens, Katerina Harvati, Nicholas J. Conard, Wolfgang Haak, Adam Powell, and Johannes Krause

Supplemental Data

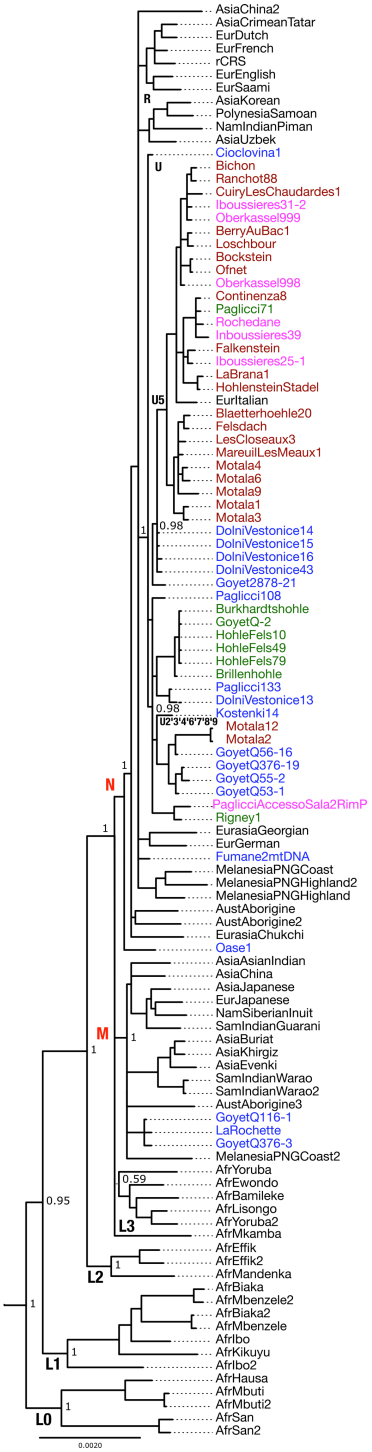

Figure S1.

Bayesian phylogenetic tree of 54 present-day human and 55 Pre-Neolithic mtDNA genomes (related to Figure 2). The tree shows the same general topology of the Maximum Parsimony tree (Figure 2) with posterior probability of 1 at both M and N nodes. Pre-LGM samples are shown in blue, Post-LGM in green, Late Glacial in magenta, Holocene hunter-gatherers in red. Oase1 represents a pre-N lineage.

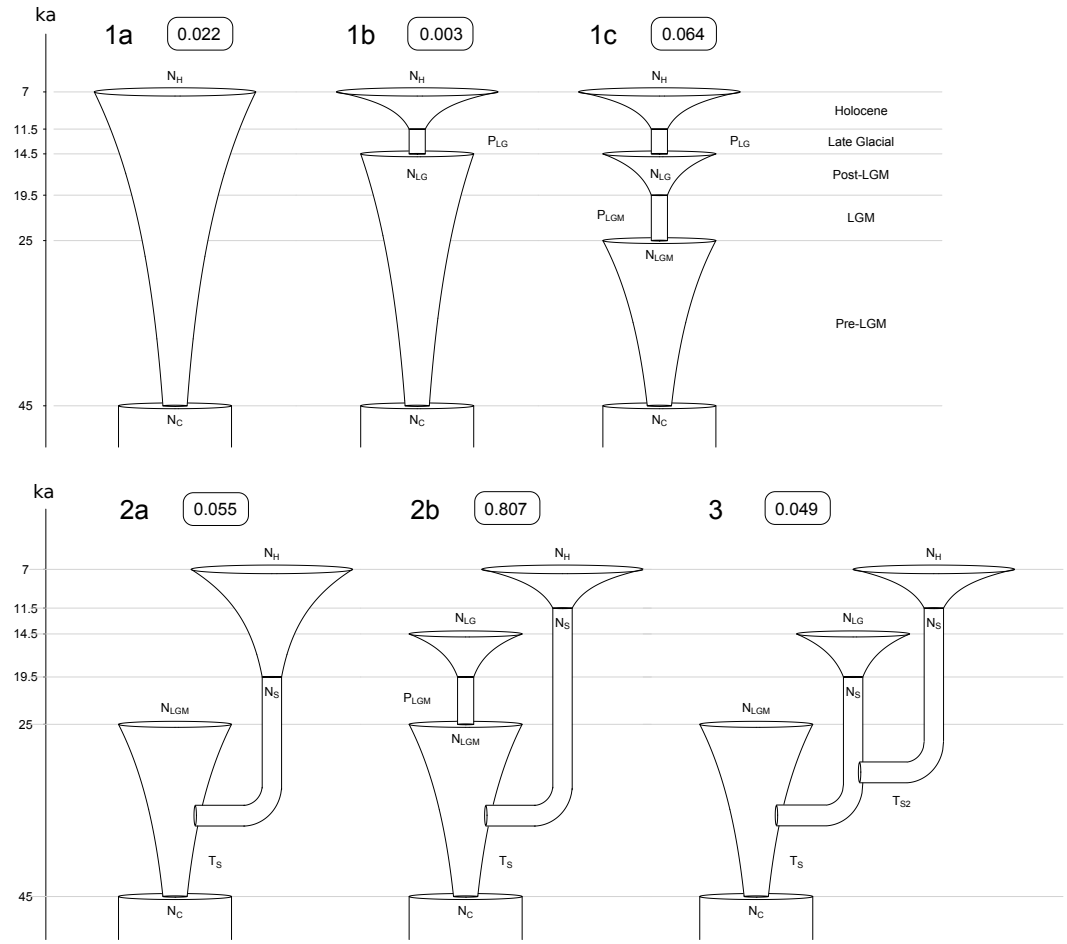

Figure S2.

Schematic of the demographic models used for coalescent simulations (related to Figure 3). The six named demographic models described in the Supplemental Experimental Procedures, with estimated model posterior probabilities given in the box in each subplot. Model 2b is identified as by far the best-fitting model, suggesting that the European hunter-gatherer population survived through an LGM bottleneck but was then largely replaced during the Late Glacial around 14.5 ka.

Table S1.

Archeological sample information (related to Figure 1). For each sample genetically analyzed, the origin, anatomical element, radiocarbon date and culture are reported (see "Archeological site information" in Supplemental Experimental Procedures). * Direct: radiocarbon date of the individual genetically analyzed; Layer: radiocarbon date of the associated stratigraphic layer.

Sample ID	Inventory name	Site (location)	Country	Geographical coordinates	Element	Date 14C (years BP) *	Source dating	Associated Culture
BerryAuBac1	BRB-1 (BVT 353)	Le Vieux Tordoir (Berry-au-Bac)	France	N 49° 24' E 03° 54'	Radius	6325±35(SacA-5455) direct	This study	Mesolithic
Bockstein	Varia I.1	Bockstein Höhle	Germany	N 48° 33' E 10° 09'	Tooth	7350±70 (UtC-7887) - 7460±60 (UtC-6796) layer	[S1]	Mesolithic
Brillenhohle	OSUT 5827	Brillenhöhle	Germany	N 48° 24' E 09° 46'	Cranium	12470±65 (OxA11054)- 12535±50 (OxA23414) direct	[S2]	Magdalenian
Burkhardtshohle	Tü 33/32 420	Burkhardtshöhle	Germany	N 48° 32' E 09° 35'	Cranium	12450±110 (ETH-7613) direct	[S3]	Magdalenian
Cioclovina1	Cioclovina1	Peştera Cioclovina Uscata˘	Romania	N 45° 35' E 23° 08'	Cranium	28510±170 (OxA-15527) direct	[S4]	Unassigned
CuiryLesChaudardes1	CRC-1	Les Fontinettes (Cuiry-lès-Chaudardes)	France	N 49° 23' E 03° 46'	Tibia	7400±60 (GrA-28268) direct	This study	Mesolithic
DolniVestonice16	DV 16	Dolní Věstonice	Czech Republic	N 48° 53' E 16° 39'	Femur	25740±210 (GrN15277) - 25570±280 (GrN15276) layer	[S5]	Gravettian
DolniVestonice43	DV 43	Dolní Věstonice	Czech Republic	N 48° 53' E 16° 39'	Femur	25740±210 (GrN15277) - 25570±280 (GrN15276) layer	[S5]	Gravettian
Falkenstein	OSUT 2306	Falkensteiner Höhle	Germany	N 48° 06' E 09° 04'	Fibula	8185±80 (ETH-7615) direct	[S6]	Mesolithic
Felsdach	F-I 28	Felsdach Inzigofen	Germany	N 48° 04' E 09° 10'	Tooth	7770 ± 120 (B-933) layer	[S7]	Mesolithic
Goyet2878-21	2878-21	Troisième caverne (Goyet)	Belgium	N 50° 26' E 05° 00'	Clavicle	22360±110 (GrA-62455) direct	This study	Gravettian
GoyetQ-2	Q-2	Troisième caverne (Goyet)	Belgium	N 50° 26' E 05° 00'	Humerus	12650±50 (GrA-46168) direct	This study	Magdalenian
GoyetQ116-1	Q116-1	Troisième caverne (Goyet)	Belgium	N 50° 26' E 05° 00'	Humerus	30880 +170, -160 (GrA-46175) direct	This study	Aurignacian
GoyetQ376-19	Q376-19	Troisième caverne (Goyet)	Belgium	N 50° 26' E 05° 00'	Humerus	23260 +110, -100 (GrA-54026) direct	This study	Gravettian
GoyetQ376-3	Q376-3	Troisième caverne (Goyet)	Belgium	N 50° 26' E 05° 00'	Humerus	29370 +180, -170 (GrA-60034) direct	This study	Aurignacian
GoyetQ53-1	Q53-1	Troisième caverne (Goyet)	Belgium	N 50° 26' E 05° 00'	Fibula	23920±100 (GrA-46169) direct	This study	Gravettian
GoyetQ55-2	Q55-2	Troisième caverne (Goyet)	Belgium	N 50° 26' E 05° 00'	Fibula	23270 +120, -110 (GrA-54031) direct	This study	Gravettian
GoyetQ56-16	Q56-16	Troisième caverne (Goyet)	Belgium	N 50° 26' E 05° 00'	Fibula	22100±100 (GrA-59991) direct	This study	Gravettian
HohleFels10	HF 10 Ic 405	Hohle Fels	Germany	N 48° 22' E 09° 45'	Femur	12770±220 (H5312-4907) - 13085±95 (H5119-4601) layer	[S8]	Magdalenian
HohleFels49	HF 49 Ib1 66	Hohle Fels	Germany	N 48° 22' E 09° 45'	Femur	12770±220 (H5312-4907) - 13085±95 (H5119-4601) layer	[S8]	Magdalenian
HohleFels79	HF 79 IIb 876	Hohle Fels	Germany	N 48° 22' E 09° 45'	Cranium	12490±70 (MAMS-25564) direct	This study	Magdalenian
HohlensteinStadel	OSUT 5830 a-c	Hohlenstein-Stadel	Germany	N 48° 32' E 10° 10'	Vertebra	7835±80 (ETH-5732) direct	[S9]	Mesolithic
Iboussieres25-1	IBS-6 (25-1)	Aven des Iboussières (Malataverne)	France	N 44° 29' E 04° 45'	Coxal	10140±50 (GrA-43700) layer	This study	Epipaleolithic
Iboussieres31-2	IBS-8 (31-2)	Aven des Iboussières (Malataverne)	France	N 44° 29' E 04° 45'	Vertebra	10140±50 (GrA-43700) layer	This study	Epipaleolithic
Iboussieres39	IBS-9 (39)	Aven des Iboussières (Malataverne)	France	N 44° 29' E 04° 45'	Femur	10140±50 (GrA-43700) direct	This study	Epipaleolithic
LaRochette	OSUT 7074	La Rochette (saint Léon-sur-Vézère)	France	N 45° 00' E 01° 05'	Ulna	23630±130 (OxA11053)- 23400±110 (OxA23413) direct	[S2]	Gravettian
LesCloseaux3	LCX-13 (s3 b1)	Les Closeaux (Rueil-Malmaison)	France	N 48° 52' E 02° 11'	Femur	8870±130 (OxA-7109(Ly-612)) direct	[S10]	Mesolithic
MareuilLesMeaux1	MLM-1 (burial 11)	Les Vignolles (Mareuil-lès-Meaux)	France	N 48° 55' E 02° 51'	Femur	8320±90 (GrN-27225) direct	[S10]	Mesolithic
Ofnet	OSUT 4043	Große Ofnet Höhle	Germany	N 48° 49' E 10° 27'	Tooth	7480±80(OxA1574) layer	[S9]	Mesolithic
Paglicci108	PA108 (21B-1)	Grotta Paglicci	Italy	N 41° 40' E 15° 34'	Phalanx	23470±370 (F-52) layer	[S11]	Gravettian
Paglicci133	PA133 (23C-2)	Grotta Paglicci	Italy	N 41° 40' E 15° 34'	Tooth	28100±400 (UTC-1414) - 29300±600(UtC-1789) layer	[S12]	Gravettian
Paglicci71	PA71 (8A)	Grotta Paglicci	Italy	N 41° 40' E 15° 34'	Patella	15460±220 (F-66) layer	[S13]	Epigravettian
Ranchot88	RAN88D9AOC154	L'abri des "Cabônes"	France	N 47° 09' E 05° 43'	Cranium	8985±40 (GrA-38019) direct	This study	Mesolithic
Rigney1	Rigney 1	Rigney 1 (Rigney)	France	N 47° 23' E 06° 10'	Mandible	12930 ± 55 Ly-6515 (OxA) direct	[S14]	Magdalenian
Rochedane	RochedaneA' 69	Rochedane (Villars-sous-Dampjoux)	France	N 47° 20' E 06° 45'	Mandible	11120±50 (GrA-41739) direct	[S14]	Epipaleolithic

Table S2.

Summarized mtDNA capture results (related to Figure 1 and Figure 2). Schmutzi [S15] output comprising mtDNA average coverage, average length, deamination at molecule termini, contamination estimate. MtDNA haplogroup was assigned with Haplogrep. The last column provides the number of unassigned positions (Ns) over the complete mtDNA (16569bp).

Sample ID	Library ID	mtDNA (fold)	Insert size (bp)	5' deamination (%)	3' deamination (%)	contamination estimate (%), first iteration (low - high)	contamination estimate (%), final iteration (low - high)	mtDNA haplogroup	Ns (bp)
BerryAuBac1	GA261	106.8	55.4	59.5	57.6	5.5 (5 - 6)	1 (0 - 2)	U5b1a	1
Bockstein	GA89	267.0	50.4	32.4	32.5	6 (5.5 - 6.5)	1 (1 - 1)	U5b1d1	1
Brillenhohle	GA79	18.6	54.4	23.6	22.2	29.5 (27.5 - 31.5)	4 (3 - 5)	U8a	64
Burkhardtshohle	Burk	45.0	65.5	30.6	30.8	29.5 (28.5 - 30.5)	13 (12 - 14)	U8a	1
Cioclovina1	Cioclovina	19.2	64.6	26.3	23.5	28 (26 - 30)	3 (2 - 4)	U	2
CuiryLesChaudardes1	GA113	16.9	54.3	60.4	55.8	4.5 (3.5 - 5.5)	1 (0 - 2)	U5b1b	2
DolniVestonice16	DV16	14.5	80.9	27.3	29.0	26 (23.5 - 28.5)	1 (0 - 2)	U5	30
DolniVestonice43	DV43	46.3	57.0	46.0	44.4	12 (11 - 13)	1 (0 - 2)	U5	1
Falkenstein	FL	599.7	56.1	37.0	37.1	4 (3.5 - 4.5)	1 (1 - 1)	U5b2a	1
Felsdach	Fels	55.2	50.6	33.7	34.2	28 (27.5 - 28.5)	13 (12 - 14)	U5a2c	17
Goyet2878-21	GA232	21.1	54.4	31.8	32.1	21.5 (20 - 23)	3 (2 - 4)	U5	12
GoyetQ-2	GA231	406.0	49.8	38.0	36.7	10.5 (10 - 11)	1 (1 - 1)	U8a	0
GoyetQ116-1	GA63	56.0	54.3	29.2	28.9	14 (13 - 15)	2 (2 - 2)	M	3
GoyetQ376-19	Q376-19	42.8	52.2	37.3	35.1	15.5 (14.5 - 16.5)	4 (3 - 5)	U2	3
GoyetQ376-3	Q376-3	45.7	60.6	24.8	23.2	31 (30 - 32)	12 (11 - 13)	M	1
GoyetQ53-1	Q53-1	48.3	60.6	31.5	31.9	25.5 (24.5 - 26.5)	12 (11 - 13)	U2	2
GoyetQ55-2	Q55-2	17.0	76.8	22.2	23.6	42 (40 - 44)	10 (8 - 12)	U2	31
GoyetQ56-16	Q56-16	45.1	72.6	22.2	24.5	36.5 (35.5 - 37.5)	4 (4 - 4)	U2	1
HohleFels10	GA81	106.2	52.0	40.0	41.1	7.5 (7 - 8)	1 (0 - 2)	U8a	1
HohleFels49	GA82	364.2	64.9	35.9	36.1	11 (10.5 - 11.5)	1 (1 - 1)	U8a	0
HohleFels79	GA90	42.2	52.2	33.7	32.7	22 (21 - 23)	3 (3 - 3)	U8a	1
HohlensteinStadel	VE	33.5	59.4	25.8	20.9	26.5 (25.5 - 27.5)	16 (15 - 17)	U5b2c1	1
Iboussieres25-1	MA121	27.1	73.6	40.7	41.7	11 (9.5 - 12.5)	4 (3 - 5)	U5b2a	2
Iboussieres31-2	MA123	13.6	68.0	44.2	42.7	19 (17 - 21)	4 (3 - 5)	U5b1	4
Iboussieres39	GA77	30.9	49.7	61.1	59.7	9.5 (8.5 - 10.5)	3 (2 - 4)	U5b2b	1
LaRochette	LaRochette	40.1	55.7	31.9	31.6	24 (23 - 25)	14 (13 - 15)	M	2
LesCloseaux3	LCX	19.0	62.9	39.4	37.2	28 (26.5 - 29.5)	12 (10 - 14)	U5a2	3
MareuilLesMeaux1	MLM	18.9	63.8	44.7	40.0	31 (29.5 - 32.5)	16 (14 - 18)	U5a2	5
Ofnet	GA93	1859.3	53.4	31.1	30.4	9.5 (9 - 10)	1 (1 - 1)	U5b1d1	0
Paglicci108	B1	19.5	54.4	45.0	34.2	21.5 (20 - 23)	6 (5 - 7)	U2'3'4'7'8'9	4
Paglicci133	C2	27.7	51.4	54.4	53.3	17.5 (16.5 - 18.5)	7 (6 - 8)	U8c	6
Paglicci71	FA	11.6	52.8	60.0	60.6	10.5 (9 - 12)	5 (4 - 6)	U5b2b	23
Ranchot88	GA262	86.3	47.7	53.7	49.4	0 (0 - 0.5)	4 (3 - 5)	U5b1	1
Rigney1	Rigney1	41.4	62.4	32.8	30.6	26 (25 - 27)	10 (9 - 11)	U2'3'4'7'8'9	1
Rochedane	GA127	104.4	47.8	42.7	43.4	12 (11.5 - 12.5)	1 (0 - 2)	U5b2b	1

Table S3.

Dated ancient mtDNA genomes (related to Table 1). 66 ancient radiocarbon dated samples (except the archeologically dated Stuttgart sample) used as calibration points in BEAST [S16] to estimate the mtDNA molecular clock. *^{14}C dates newly reported in this study were calibrated using Reimer et al. [S17] calibration curve and reported in calibrated years before present (cal BP).

Sample ID	Country	Date interval (cal BP)*	Data source
Ajvide52	Sweden	4600-4900	[S18]
Ajvide58	Sweden	4600-4900	[S18]
Ajvide70	Sweden	4600-4900	[S18]
BerryAuBac1	France	7169-7319	This study
BLA10*	Germany	5355-5481	[S19]
BLA11*	Germany	5862-5982	[S19]
BLA13*	Germany	5411-5615	[S19]
BLA14*	Germany	5589-5617	[S19]
BLA20*	Germany	10594-10710	[S19]
BLA7*	Germany	5646-5686	[S19]
Bockstein	Germany	8016 - 8329	This study
Boshan11	China	8040-8320	[S20]
BRA1	Spain	7690-7940	[S21]
Brillenhohle	Germany	14440-15120	This study
Burkhardtshohle	Germany	14150 – 15080	This study
Cioclovina1	Romania	32519-33905	This study
CuiryLesChaudardes1	France	8050-8360	This study
DolniVestonice13	Czech Republic	31070-31240	[S20]
DolniVestonice14	Czech Republic	31070-31240	[S20]
DolniVestonice16	Czech Republic	29386 - 30567	This study
Falkenstein	Germany	8993 - 9409	This study
Felsdach	Germany	8380-8980	This study
Fumane2	Italy	38500-41110	[S22]
Gökhem2	Sweden	4750-5050	[S18]
Gökhem5	Sweden	4750-5050	[S18]
Gökhem7	Sweden	4750-5050	[S18]
Goyet2878-21	Belgium	26269 - 27055	This study
GoyetQ-2	Belgium	14780-15230	This study
GoyetQ116-1	Belgium	34430-35160	This study
GoyetQ376-19	Belgium	27310-27720	This study
GoyetQ376-3	Belgium	33140-33940	This study
GoyetQ53-1	Belgium	27720-28230	This study
GoyetQ55-2	Belgium	27310-27730	This study
GoyetQ56-16	Belgium	26040-26600	This study
HohleFels49	Germany	15568 - 16250	This study
HohleFels79	Germany	14270-15070	This study
HohlensteinStadel	Germany	8446 - 8809	This study
Iboussieres39	France	11600-12040	This study
Iceman	Italy	5100-5350	[S23]
Ire8	Sweden	4150-5100	[S18]
Kostenki14	Russia	37320-38650	[S24]
LaRochette	France	27400-27784	This study
LesCloseaux3	France	9580-10230	This study
Loschbour	Luxembourg	7927-8181	[S25]
MA-1	Russia	23891-24423	[S26]
MareuilLesMeaux1	France	9080-9500	This study
Motala1	Sweden	7530-8375	[S25]
Motala12	Sweden	7530-8375	[S25]
Motala2	Sweden	7530-8375	[S25]
Motala3	Sweden	7530-8375	[S25]
Motala4	Sweden	7530-8375	[S25]
Motala6	Sweden	7530-8375	[S25]
Motala9	Sweden	7530-8375	[S25]
Oase1	Romania	37000-42000	[S27]
Oberkassel998	Germany	13870-14170	[S20]
Oberkassel999	Germany	13290-13570	[S20]
Ofnet	Germany	8159 - 8424	This study
Paglicci108	Italy	27831 – 28961	This study
Paglicci71	Italy	18197-18973	This study
Ranchot88	France	9933-10235	This study
Rigney1	France	15240-15690	This study
Rochedane	France	12830-13090	This study
Saqqaq	Greenland	3600-4170	[S28]
Stuttgart	Germany	6800-7150	[S25]
Tianyuan1301	China	38830-40120	[S20]
Ust'Ishim	Russia	43210-46880	[S29]

Table S4.

European pre-Neolithic dated mtDNA genomes (related to Figure 1 and Figure 3). 55 complete or almost complete mtDNA sequences of Late Pleistocene and early Holocene hunter-gatherers (sorted chronologically) used for coalescent demographic modeling. The last column provides average values of ^{14}C-dates reported in calibrated years before present (cal BP). ^Radiocarbon date not available in the study.

Sample ID	Country	Map sites (Figure 1)	Time period	Haplogroup	Publication	Date (cal BP)
Fumane2	Italy	Fumane	preLGM	R	[S22]	39805
Kostenki14	Russia	Kostenki	preLGM	U2	[S24]	37985
GoyetQ116-1	Belgium	Goyet	preLGM	M	This study	34795
GoyetQ376-3	Belgium	Goyet	preLGM	M	This study	33540
Cioclovina1	Romania	Cioclovina	preLGM	U	This study	33212
Paglicci133	Italy	Paglicci	preLGM	U8c	This study	33000
DolniVestonice13	Czech Republic	Dolni Vestonice	preLGM	U8	[S20]	31155
DolniVestonice14	Czech Republic	Dolni Vestonice	preLGM	U5	[S20]	31155
DolniVestonice15	Czech Republic	Dolni Vestonice	preLGM	U5	[S20]	31155
DolniVestonice16	Czech Republic	Dolni Vestonice	preLGM	U5	This study	29977
DolniVestonice43	Czech Republic	Dolni Vestonice	preLGM	U5	This study	29977
Paglicci108	Italy	Paglicci	preLGM	U2'3'4'7'8'9	This study	28396
GoyetQ53-1	Belgium	Goyet	preLGM	U2	This study	27975
LaRochette	France	La Rochette	preLGM	M	This study	27592
GoyetQ55-2	Belgium	Goyet	preLGM	U2	This study	27520
GoyetQ376-19	Belgium	Goyet	preLGM	U2	This study	27515
Goyet2878-21	Belgium	Goyet	preLGM	U5	This study	26662
GoyetQ56-16	Belgium	Goyet	preLGM	U2	This study	26320
Paglicci71	Italy	Paglicci	postLGM	U5b2b	This study	18585
HohleFels79	Germany	Swabian Jura	postLGM	U8a	This study	15909
HohleFels10	Germany	Swabian Jura	postLGM	U8a	This study	15470
HohleFels49	Germany	Swabian Jura	postLGM	U8a	This study	15470
Rigney1	France	French Jura	postLGM	U2'3'4'7'8'9	This study	15465
GoyetQ-2	Belgium	Goyet	postLGM	U8a	This study	15005
Brillenhohle	Germany	Swabian Jura	postLGM	U8a	This study	14780
Burkhardtshohle	Germany	Swabian Jura	postLGM	U8a	This study	14615
Oberkassel998	Germany	Oberkassel	LateGlacial	U5b1	[S20]	14020
Bichon	Switzerland	French Jura	LateGlacial	U5b1h	[S30]	13700
Oberkassel999	Germany	Oberkassel	LateGlacial	U5b1	[S20]	13430
Paglicci Accesso sala 2 Rim P	Italy	Paglicci	LateGlacial	U2'3'4'7'8'9	[S20]	13000^
Rochedane	France	French Jura	LateGlacial	U5b2b	This study	12960
Iboussieres39	France	Aven des Iboussières	LateGlacial	U5b2b	This study	11820
Iboussieres25-1	France	Aven des Iboussières	LateGlacial	U5b2a	This study	11820
Iboussieres31-2	France	Aven des Iboussières	LateGlacial	U5b1	This study	11820
BLA20*	Germany	Blätterhöhle	Holocene	U5a2c3*	[S19]	10652
Ranchot88	France	French Jura	Holocene	U5b1	This study	10084
Continenza 8	Italy	Continenza	Holocene	U5b2b1	[S20]	10000^
LesCloseaux3	France	Paris Basin	Holocene	U5a2	This study	9905
MareuilLesMeaux1	France	Paris Basin	Holocene	U5a2	This study	9290
Falkenstein	Germany	Swabian Jura	Holocene	U5b2a	This study	9201
Felsdach	Germany	Swabian Jura	Holocene	U5a2c	This study	8680
HohlensteinStadel	Germany	Swabian Jura	Holocene	U5b2c1	This study	8628
Ofnet	Germany	Swabian Jura	Holocene	U5b1d1	This study	8292
CuiryLesChaudardes1	France	Paris Basin	Holocene	U5b1b	This study	8205
Bockstein	Germany	Swabian Jura	Holocene	U5b1d1	This study	8173
Loschbour	Luxembourg	Loschbour	Holocene	U5b1a	[S20]	8054
Motala1	Sweden	Motala	Holocene	U5a1	[S25]	7953
Motala12	Sweden	Motala	Holocene	U2e1	[S25]	7953
Motala2	Sweden	Motala	Holocene	U2e1	[S25]	7953
Motala3	Sweden	Motala	Holocene	U5a1	[S25]	7953
Motala4	Sweden	Motala	Holocene	U5a2d	[S25]	7953
Motala6	Sweden	Motala	Holocene	U5a2d	[S25]	7953
Motala9	Sweden	Motala	Holocene	U5a2	[S25]	7953
BRA1	Spain	La Braña	Holocene	U5b2c1	[S21]	7815
BerryAuBac1	France	Paris Basin	Holocene	U5b1a	This study	7244

Table S5.

ABC estimated parameter posterior distributions for demographic model 2b in Figure S2 (related to Figure 3). Prior distributions are given, along with modes, medians and 95% highest posterior density (HPD) intervals for each parameter. Tolerance proportion $F\delta = 0.25\%$, i.e. 12500 retained from 5 million simulations. Prior distributions for the two additional parameters used in other models are given in gray.

	Prior (uniform)				HPD	
Parameter	**Minimum**	**Maximum**	**Mode**	**Median**	**2.5%**	**97.5%**
$\log(N_C)$	1	3.699	1.963	1.867	1.057	3.113
T_S	45 ka	25 ka	29394	29610	36420	25000
$\log(N_S)$	2	4.699	3.099	3.148	2.762	3.767
$\log(N_{LGM})$	2	4.699	3.329	3.202	2.248	4.036
P_{LGM}	0	1	0.169	0.305	0.074	0.909
$\log(N_{LG})$	2.699	4.699	2.802	3.048	2.713	4.407
$\log(N_H)$	2.699	5	4.265	4.062	2.871	4.928
T_{S2}	T_S	19.5 ka	-	-	-	-
P_{LG}	0	1	-	-	-	-

Table S6.

Summary statistics (related to Figure 3). Observed statistic values, ranked by median Kruskal-Wallis p-value per block for ABC model choice. Sample groups: 0 = Holocene; 1 = Late Glacial; 2 = Post-LGM; and 3 = Pre-LGM. h_i = number of haplotypes; H_i = haplotype diversity; π_i = mean number of pairwise differences; s_i = number of polymorphic sites; D_i = Tajima's D. Within-group statistics for the Pre-LGM sample group (group 3), in gray are excluded from the model choice procedure, as described in the Supplemental Experimental Procedures.

Summary statistic	Observed value	Kruskal Wallis test p-value
h_0	19	
h_1	7	~0
h_2	4	
h_3	15	
H_0	0.943	
H_1	0.857	~0
H_2	0.563	
H_3	0.930	
π_{0vs1}	14.211	
π_{0vs2}	19.470	
π_{0vs3}	19.104	~0
π_{1vs2}	17.714	
π_{1vs3}	19.286	
π_{2vs3}	16.680	
$F_{ST\ 0vs1}$	0.069	
$F_{ST\ 0vs2}$	0.415	
$F_{ST\ 0vs3}$	0.258	~0
$F_{ST\ 1vs2}$	0.416	
$F_{ST\ 1vs3}$	0.319	
$F_{ST\ 2vs3}$	0.323	
s_{all}	145	1E-301
π_{all}	16.776	1E-301
π_0	14.262	
π_1	12.191	5.052E-276
π_2	8.500	
π_3	14.083	
s_0	77	
s_1	36	4.999E-264
s_2	29	
s_3	54	
D_0	-1.349	
D_1	-0.977	2.771E-130
D_2	-1.271	
D_3	-0.572	
H_{all}	0.971	3.49E-128
h_{all}	45	8.310E-113
D_{all}	-1.704	1.840E-81

Supplemental Experimental Procedures

Ancient DNA

Sampling
Human specimens under investigation for ancient DNA (aDNA) (Table S1) were brought to "clean room" facilities at the Institute for Archaeological Sciences in Tübingen, cataloged (Sample ID assignment), photographed (and in presence of diagnostic morphological features also surface scanned) and stored in sample plastic bags. If not already powdered, both bones and teeth were irradiated for at least 1 hour under UV lights before starting with sample processing. Teeth were sampled by cutting each tooth transversally with a coping saw under the crown/root border in order to not damage informative enamel characteristics. Tooth dentine from inside either dental crowns or roots was powdered using a dentist drill with diamond bits rotated at low speed (below 15rpm). For bone sampling, the dentist drill was used with the same settings, initially to remove a thin layer of surface, and then to drill inside the bone. For each specimen between 30 mg and 120 mg of bone/tooth powder were sampled and used in DNA extraction.

DNA extraction and library preparation
DNA was extracted from bone and tooth powder following a published method especially designed for the retrieval of short DNA fragments typical of aDNA [S31], except for the samples DolniVestonice16 and DolniVestonice43 that were extracted with a different silica-based protocol [S32]. DNA was eluted in 100µl TET (10mM Tris-HCl, 1mM EDTA pH 8.0, 0.1% Tween20) and between 5 µl and 60 µl of DNA extract was transformed into a genetic library following a double stranded DNA protocol without any UDG treatment in order to keep damage pattern along DNA fragments [S33]. The concentration of not indexed libraries measured with qPCR varied form ~10E8 to ~10E9 copies/ul whereas extraction and library negative controls show 4 to 5 orders of magnitude lower concentration (not shown). Moreover, extraction and library positive controls (cave bear specimens) resulted in expected concentrations confirming the extraction and library preparation success. A unique combination of two indexes (6-8 base pair (bp)) was incorporated in each library molecule as sample specific DNA barcodes [S34]. Library aliquots before and after 10 cycles of indexing PCR were quantified with qPCR [S33] and the reactions success were estimated as total molecules after indexing over total molecules before indexing. Indexed libraries of each sample were subsequently amplified for different PCR cycles with AccuPrime Pfx DNA polymerase as reported in Schuenemann et al. [S35] in order to stay below the reaction plateau phase and avoid heteroduplex formation [S36]. Extraction and library negative controls were treated accordingly. Amplified products were then purified using MinElute spin columns following the manufacturer's protocol and quantified on an Agilent 2100 Bioanalyzer DNA 1000 chip.

Mitochondrial DNA enrichment and sequencing
Human mitochondrial DNA (mtDNA) was enriched through a bait-capture method described in Maricic et al. [S37]. Up to five amplified indexed libraries from different samples were pooled equimolarly to reach a total of 2000ng DNA and captured together. Hybridized molecules were eluted from streptavidin beads with 125mM NaOH and purified on MinElute spin columns. After qPCR quantification, pooled captured libraries yielded a concentration between ~10E5 (blanks) and ~10E7 copies/ul. A positive control library with known mtDNA preservation was captured in parallel to estimate the efficiency of the enrichment process. An additional amplification with AccuPrime Pfx DNA polymerase of each pool was performed as mentioned before. Enriched library pools were then quantified using an Agilent 2100 Bioanalyzer DNA 1000 chip, pooled in equal concentration and sequenced in different percentage on several HiSeq2500 via 2x100+8+8 cycles and an Illumina MiSeq run for 2x150+8+8 cycles. After sequencing, libraries yielded between 1 and 10 million reads.

DNA sequence pre-processing and mapping
Base call files (.bcl) were calculated by the Instrument Control Software's RTA, which employs Bustard as base caller [S38]. Bcl were converted in raw sequences that were demultiplexed and sorted in sample specific folders making use of the individual double barcodes. First, adaptors and index sequences were clipped off. Paired-end reads were then merged into single sequences if they overlapped by at least 10bp and choosing the base with higher sequencing quality if forward and reverse read disagreed [S39]. Only merged reads above 30bp length were mapped. Alignment of the selected sequences to the human

mitochondrial genome reference (rCRS) was performed using BWA with "–n 5" parameter [S40] in combination with a custom developed tool that takes into account the circularity of mtDNA [S41] and between ~0.2 and 50% of reads were mapped. After mapping, duplicate sequences with the same start and end positions were removed using a tool developed in-house that considers coordinates of both read termini [S41]. Reads with mapping quality below 30 were discarded with the samtools software package [S42] in order to consider only sequences with a secure placement within the mtDNA in subsequent analyses. Finally, we obtained an average coverage of mtDNA ranging between 11 and 1860-fold with an average fragment length of 49 to 80bp and deamination rate at read termini from 20 to 61% (Table S2).

Joint consensus call and contamination estimates

A probabilistic iterative method, schmutzi [S15], was used (parameters: "--logindel 1 --uselength") to jointly infer the endogenous consensus and to estimate present-day human contamination levels. Average deamination rates at the first bases of the 5' and 3' ends were computed using internal programs that are part of the software package. The program mitigates the impact of deamination on consensus calling. To identify endogenous bases, the software uses deamination rates and sequence length distributions of the fragments. Present-day human contamination estimates were performed using a non-redundant database of human mitochondrial genomes distributed with the software package. An initial contamination estimate was computed using deamination patterns. Since these contaminating DNA fragments can be longer than endogenous aDNA ones, there can be a discrepancy between a contamination estimate based on the fraction of contaminating fragments versus one based on the fraction of contaminating bases. Since the initial contamination estimate based on deamination patterns produces an estimate more consistent with the former definition, this estimate is refined in later iterations of the program to facilitate endogenous consensus calling as it relies on the latter definition. These subsequent iterations use the endogenous consensus and the aforementioned database of putative mitochondrial contaminant genomes. This method iteratively co-estimates the endogenous mitochondrial genome and the present-day human contamination rate. The predicted endogenous bases and insertions/deletions are produced with an error probability on a PHRED scale. Due to the relatively low coverage for some samples, no quality threshold was applied on the final predictions thus effectively taking the bases with the highest posterior probability. The following poly-C regions and mutational hotspot were masked on the final endogenous consensus sequence: 303-315, 515-522, 16519 [S43]. The resulting sequences were uploaded to HaploGrep [S44] to assign haplogroups and call mtDNA SNPs against the Reconstructed Sapiens Reference Sequence (RSRS) [S45] (Table S2).

Visual inspection and haplotype calls

Given the significance of the samples but also critical levels of contamination detected in some of them using schmutzi, we also inspected each assembly visually and made phylogeny informed haplotype calls for both the assumed endogenous portion of reads (the majority of damaged reads) and contaminating lineages that were identified by characteristic substitution profiles. The standardized procedure is described as follows:

i. We imported the bam.files into Geneious 8.1.7 (http://www.geneious.com) [S46] and re-assembled the reads against the Reconstructed Sapiens Reference Sequence (RSRS) [S45] with 5 iterations, which improved the assembly in problematic C-stretch regions of the HVS I and II.

ii. We used the automated variant caller of Geneious with a minimum variant frequency of 0.7 (or 0.6 for samples with high contamination), and a minimum coverage of 2X and exported the resulting variant (SNP) tables into Excel.

iii. We compared the variants to the SNPs reported in the online mtDNA phylogeny (mtDNA tree Build 16, 19 Feb 2014, http://www.phylotree.org) to ensure all phylogenetically expected SNPs are indeed observed. As per above, we masked notoriously troublesome sites at 309.1C(C), 315.1C, AC indels at 515-522, 16182C, 16183C, 16193.1C(C) and 16519 [S43].

iv. The assemblies were subsequently inspected visually, taking note of additional SNPs that might be presented but had been called automatically as the variant frequency fell below the 0.7 (0.6) cut-off. At the same time we paid particular attention to sites that could identify potential contaminating lineages. For example, as both ancient and contaminating lineages are in all cases of Eurasian origin, SNPs of the basal 'African' stem of the tree are shared and therefore present in nearly 100% of all reads covering the respective sites. For most samples (non-M haplogroup), this was also the case for the characteristic SNPs leading into macro-hg N (G8701A, C9540T, G10398A, C10873T, A15301G!), and R (T12705C, T16223C). For all reads covering SNP sites characteristic for hg U (A11467G, A12308G, G12372A) and

the respective diagnostic U sub-hg SNPs we usually also observed a fraction of reads that did not show the derived status at these sites. If the ratio of 'contaminating' reads exceeded 5%, it proved relatively easy to track down the profile of the contaminating lineage, for example by double-checking for reads with derived calls in diagnostic SNP sites for hg H (G73A, A11719G, T14766C, G2706A, T7028C). An alternative crude but effective check was to look at the HVSI regions for SNPs that are characteristic for other haplogroups (which often proved to be a reliable indicator) and then checking the expected diagnostic positions from the last common branch (in most cases branch R) upwards.

v. For these diagnostic sites we simply counted the number of ancestral and derived bases relative to the depth of coverage at that site. By averaging across all diagnostic sites that lead from the common branch R to a derived sub-haplogroup (e.g. 12 sites for sub-hg U5a1 or 5 sites into basal hg H), we have sufficient data points to calculate a rough but direct estimate for the support (majority or minority) of the respective lineages present in reads from an ancient sample, which is also a direct measure of support of endogenous vs. contaminating reads. For example, sample Paglicci108 is very likely a U2'3'4'7'8'9 lineage but the derived diagnostic SNPs are only present in 67.4% of the reads on average. At the same time, we observe reads that are derived at six characteristic SNPs diagnostic for hg H1 with an average 33.9% of the reads. This almost sums up perfectly, while the discrepancy could be explained by DNA damage that could potentially confound the precision of the signal by in- or deflating the calls for SNP, which follow the direction (C>T, G>A) of characteristic ancient DNA damage. Moreover, the authenticity of the mtDNA hg U2'3'4'7'8'9 rather than H1 is further confirmed by the coalescence age of the latter hg being considerably younger (~10 ka) [S45] than the age of the specimen (~ 28ka).

The SNP lists generated by schmutzi and visual inspection were finally compared for each sample and the detected inconsistencies were manually checked in the read alignments using Geneious. In total only 34 positions were edited in the schmutzi consensus sequences over the complete dataset of 35 complete mtDNAs (see below). Only 5 positions were converted into a different nucleotide based on hg phylogeny or contamination that was further estimated looking at reads also overlapping neighboring mutations. Insertions were shifted in 6 samples because of misalignment with the reference genome. Finally all the others 22 positions were mainly transitions (19 out of 22) in the form C to T or G to A that were converted into Ns because after visual inspection we couldn't rule out post-mortem-damage origin especially at low coverage (1-3fold).

For each sample we report below the assigned haplogroup (Table S2) in bold, their derived and missing SNPs compared to the RSRS reference and the manually edited positions in brackets.

- BerryAuBac1, **U5b1a**: T16192C!, C16519T
- Bockstein, **U5b1d1**: C16176T, C16519T, (525insAC)
- Brillenhohle, **U8a**: G1422A, C16519T, C9365T missing, (C14519N, 10107N, 14493N)
- Burkhardtshohle, **U8a**: C150T, G1422A, C16519T, C9365T missing, (A7055G)
- Cioclovina1, **U**: T15889C, C16519T, (G12372A)
- CuiryLesChaudardes1, **U5b1b**: 6056T, 6057T, T16092C, C16327T, C16519T, (7362N)
- DolniVestonice16, **U5**: G1462A, C16519T, (4N, 6N)
- DolniVestonice43, **U5**: T16231C, C16519T
- Falkenstein, **U5b2a**: A4732G, G8572A, A16171G, C16519T, T16189C! missing
- Felsdach, **U5a2c**: T152C!,735.1G, 11728T, C16192T, C16519T
- Goyet2878-21, **U5**: T3202C, C3612T, C13272T, A13299G, T16192C!, C16519T
- GoyetQ-2, **U8a**: C150T, G1422A, C16519T, C9365T missing
- GoyetQ116-1, **M**: G207A, C1556T, C6045T, C8619a, A11084G, T16297C
- GoyetQ376-19, **U2**: C152T!!, T217C, T5426C, G12406A, A12579G, T16092C, G16129c, T16189C!
- GoyetQ376-3, **M**: G207A, C1556T, A6040G, C6041T, C6045T, C8619a, A11084G, T16297C
- GoyetQ53-1, **U2**: C152T!!, T217C, T5426C, G12406A, A12579G, 16129G, T16189C!, (1N)
- GoyetQ55-2, **U2**: C152T!!, T217C, C4011T, C4013T, T5426C, G12406A, A12579G, T16092C, G16129c, T16189C!, (T16092C)
- GoyetQ56-16, **U2**: C152T!!, T217C, T5426C, G16129c, T16189C!, T16362C
- HohleFels10, **U8a**: C150T, G1422A, C16519T, C9365T missing
- HohleFels49, **U8a**: C150T, G1422A, C16519T, C9365T missing
- HohleFels79, **U8a**: C150T, G1422A, C16519T, C9365T missing
- HohlensteinStadel, **U5b2c1**: C16519T, (960.XC, T14182C)

- Iboussieres25-1, **U5b2a**: A4732G, C16114a, C16519T
- Iboussieres31-2, **U5b1**: 12398T, G13708A, C16519T, (6N, 11N, 16192.1T)
- Iboussieres39, **U5b2b**: 6027A, 8161T, T8167C, T13356C, C16519T
- LaRochette, **M**: G207A, C1556T, C6045T, C6164T, C8619a, A11084G, C12816T, (525insAC, 16297N)
- LesCloseaux3, **U5a2**: G54A, G7805A, C16519T
- MareuilLesMeaux1, **U5a2**: T16362C, C16519T, (6008N)
- Ofnet, **U5b1d1**: C16176T, C16519T, (525insAC)
- Paglicci108, **U2'3'4'7'8'9**: G1709A, G6260A, T9716C, C16256T, C16519T (C14766T)
- Paglicci133, **U8c**: C16519T, (6N, 11N)
- Paglicci71, **U5b2b**: C6910T, C16519T, (11N, 4467N, 5213N, 5844N, 7396N, 15050N, 16313N)
- Ranchot88, **U5b1**: G3531A,8276.1C, T16189C!, T16192C!, C16519T, (8276.1C)
- Rigney1, **U2'3'4'7'8'9**: C150T, T152C!, T6152C, T5999C, T10020C, A12082G, A12530G, G15466A, T16297C
- Rochedane, **U5b2b**: A8449G, T16086C, C16519T, (525insAC)

Phylogenetic analyses

The software MUSCLE [S47] was used to align complete or almost complete sequences of 56 Late Pleistocene and Early Holocene European human mtDNAs (including Oase1 [S27]) to 54 modern worldwide human mtDNAs [S48]. A Neanderthal mtDNA sequence (Vindija 33.25 FM865410.1) was included as a phylogenetic out-group for a total of 111 mtDNA sequences aligned. A phylogenetic tree (Figure 2) was built with the Maximum Parsimony method (SPR algorithm) using MEGA6 [S49]. The tree was constructed with 99% partial deletion for a total of 16371 positions in the final dataset. Moreover the phylogeny was tested with the bootstrap method with 1000 replications. The same multiple genome alignment, including missing sites but not gaps, was tested in Modelgenerator [S50], and GTR with invariant sites and gamma distributed correction for rate heterogeneity was found to be the substitution model that best fits the data (AIC1). This was selected in MrBayes [S51], which was used to reconstruct a Bayesian phylogenetic tree (Figure S1). Markov chain Monte Carlo (MCMC) was performed with 50,000,000 iterations and 10,000 sampling interval. After removing the first 10% of the generated trees as burn-in, the summarized tree was built, showing high posterior support at the major mitochondrial branches. Both trees were visualized and edited with FigTree v1.4.2 (http://tree.bio.ed.ac.uk/software/) and finally refined in Inkscape (https://inkscape.org/en/).

Phylogenetic relationships between 56 (55 plus Oase1) complete or almost complete mtDNA from European pre-Neolithic individuals were visualized through Maximum Parsimony and Bayesian trees, which both provided the same general topology (Figure 2, Figure S1). All ancient samples share a MRCA within the modern day mtDNA diversity with the exception of Oase1 [S27], which branches off basal to all other present-day N lineages. The great majority of samples (52 out of 55) belong to hg N mostly falling within sub-hgs U8, U5 and U2'3'4'7'8'9. Only Fumane2 [S22] represents a basal R lineage without any derived position leading to known sub-hgs, such as the ~45,000 years old individual from Ust'Ishim in Siberia [S29]. Finally, three pre-LGM individuals (LaRochette, GoyetQ116-1 and GoyetQ363-3) carry mtDNA hg M defined by four positions from the L3 split (T489C, C10400T, T14783C, G15043A). Looking more closely at the intragroup M phylogeny, these three pre-LGM individuals are all placed on a branch not yet seen in modern-day individuals, either in Europe or elsewhere. In particular GoyetQ116-1 and GoyetQ363-3 from Belgium dated ~34-35 ka, show 6 (G207A, C1556T, C6045T, C8619a, A11084G, T16297) and 8 (G207A, C1556T, A6040G, C6041T, C6045T, C8619a, A11084G, T16297) derived mutations from the M root, respectively, whereas LaRochette from South France dated ~27.5 ka presents 7 (G207A, C1556T, C6045T, C6164T, C8619a, A11084G, C12816T) derived mutations from the M root. LaRochette carries a possible additional back mutation at position C16297T! (16Ts and 4Cs), compared to the two Belgian sequences both carrying the T16297C mutation. The four Cs at this position cannot be explained by damage and are likely the result of contamination or heteroplasmy, therefore an unassigned base (N) was placed at that position in the final consensus sequence (see above). Despite their geographic and temporal separation all three pre-LGM individuals share five mutations (G207A, C1556T, C6045T, C8619a, A11084) from the MRCA of the basal M lineage. This finding suggests that this M branch arrived in Europe before 35 ka and survived at least until 27.5 ka, before the LGM started (~25 ka).

BEAST analyses

The human mtDNA mutation rate can be estimated with different methods. All rely on temporal calibration points in the past such as the split time of certain populations, assuming a known phylogeny [S45]. Ancient DNA provides the opportunity to use endogenous mtDNA of ancient radiocarbon dated specimens to tip calibrate the human mtDNA molecular clock [S20, S52]. Ancient sequences should show less derived positions than more recent ones as a sign of their antiquity because they had "less time" to accumulate mutations. Therefore sequence branch shortening can be used not only to confirm the authenticity of the results but also to date divergence events. The software package BEAST v1.8.1 [S16] was used to calculate, in a Bayesian statistic framework, the human mtDNA mutation rate with ancient dated sequences as multiple calibration points in order to estimate haplogroup divergence ages. Initially, a multiple genome alignment was performed with MUSCLE by combining 311 worldwide modern human mtDNA and 66 ancient dated mtDNAs (Table S3) for a total 377 sequences. Ancient mtDNAs were selected according to the following characteristics: i) directly ^{14}C dated specimens or associated findings or archeologically dated e.g. the early Neolithic farmer from Stuttgart; ii) excluding identical mtDNA sequences with same date; iii) over 99% of the entire mtDNA with assigned nucleotides; iv) age between ~46,800 and 3,600 years BP. After removal from the 377 mtDNA alignment of all positions containing gaps and missing data, a total of 15963 positions were retained. Modelgenerator v.85 was run indicating Tamura-Nei 93 with a fixed fraction of invariable sites and gamma distributed rates as the best-supported model for our dataset. These substitution and site heterogeneity models with 6 gamma categories were selected in BEAST. Tip dates were indicated as zero for modern sequences whereas sampling with individual priors was set for ancient sequences. For each of the 66 sequences, lower and upper values of a uniform prior distribution were given as confidence interval limits of the date estimate (Table S3). Two different models of rate variation among tree branches were investigated: a strict clock and an uncorrelated lognormal-distributed relaxed clock. In both cases an approximate continuous time Markov chain rate reference prior [S53] was chosen. Moreover, two tree priors were tested: a population Constant size and Bayesian Skyline coalescent with 20 as group number and piecewise-linear as the Skyline model. For the four different model combinations generated this way, we performed three MCMC runs with 50,000,000 iterations each, sampling every 10,000. Tracer v1.6 [S16] was used to visually inspect ESS values and chain convergence, in order to identify the percentages of each run that was discarded as chain burn-in (Table S5). For each model the three independent runs were combined using LogCombiner v1.8.1 resulting in 60,000,000 to 135,000,000 iterations and summarized in a Maximum Clade Credibility (MCC) tree using TreeAnnotator v1.8.1 (both programs included in the BEAST package). Model comparison and best support assessment was performed through a marginal likelihood estimation (MLE) using path sampling (PS) / stepping-stone sampling (SS) [S54]. Overall the Skyline tree prior resulted in higher likelihoods for both strict and relaxed molecular clock than the Constant size tree prior (Table 1). The latter provided in general older hg divergence times and a higher tree root height as previously reported [S20]. Moreover the Skyline prior, that models changes in population size through time, resulted not only in younger splitting times but also narrower confidence intervals. Despite having comparable likelihood to the strict clock, this parameter in combination with a lognormal relaxed clock required more iterations for the run to converge. A burn-in of 60% was manually selected instead of the default 10% applied for the other three combinations of parameters. This caused a strong reduction in the overall ESS values although the mutation rate and coalescence times were almost identical to the strict clock. In conclusion, the Skyline tree prior in combination with a strict clock mutation rate among different tree branches was overall best supported by the data and therefore this was favored to estimate the human mtDNA mutation rate and to assess haplogroup divergence times (Table 1).

The newly estimated mutation rate value overlapped with published rates obtained with similar methods but with a narrower confidence interval [S20, S52], possibly resulting from the higher number of calibration points used in this study. This allowed us to determine hg coalescence times more precisely especially for lineages with know rate heterogeneity, such as in the M clade [S45]. In the latter study, however, the authors reported almost identical values for hg M TMRCA (~50 ka) but an almost 10 k older hg N TMRCA (~ 59 ka) than the one we obtained. A general observation is that by using a Skyline tree prior in BEAST we allowed for changes in effective population size through time, resulting in younger mtDNA tree splits than with a Constant size tree prior (Table 5) or phylogenetic methods [S45]. However, including three Late Pleistocene M sequences as deep time anchors, gave us the opportunity to date the divergence time of all M lineages in the same way as for the N lineage. This resulted in similar TMRCAs for both N and M clades at around ~50 ka. We acknowledge the possible influence of sampling biases in our dataset of 377 ancient and modern mtDNA sequences both in terms of sample size and geographical-

temporal distribution [S55]. In order to keep the potential impact at a minimum we included a vast majority of modern worldwide mtDNAs (273 out of 311) that belong to the M and N clades. Moreover, the 66 ancient sequences represented not only European individuals before 7 ka but also mtDNAs from different regions and more recent time periods (Table S3) to reduce the aforementioned sampling biases also for the ancient sequences.

Coalescent demographic modeling with approximate Bayesian computation (ABC)

The 55 samples were divided into 4 chronologically-based sample groups: 'Pre-LGM' (~45 – 25 ka, n = 18), 'Post-LGM' (~19.5 – 14.5 ka, n = 8), 'Late Glacial' (~14.5 – 11.5 ka, n = 8) and 'Holocene' (~11.5 – 7 ka, n = 21) (Table S4). Coalescent simulations were performed using Bayes Serial Simcoal [S56], and all models assumed an intergeneration time of 25 years, a mutation rate of 2.74×10^{-8} per site per year (see main text and Table 1), a transition bias of 0.956 and a continuous gamma distribution of mutation rates across sites with parameter 0.205 [S57, S58]. We used approximate Bayesian computation (ABC) to both perform model choice [S58, S59] and estimate the parameters of the best-fitting model [S60].

Following an initial test phase, we considered six distinct demographic models: 1a, 1b, 1c, 2a, 2b and 3, illustrated schematically in Figure S2. All models start with a non-European ancestral maternal population of effective size 5000, and at 45 ka, a population of size N_C expands into Europe. In model 1a, this European population simply grows exponentially, unimpeded, up to size N_H at 7 ka. In model 1b the population grows exponentially to size N_{LG} at 14.5 ka. At this point, a Late Glacial bottleneck begins, where the population is reduced to a constant proportion P_{LG} of its current size. Following the end of the Late Glacial at 11.5 ka, the population then again grows exponentially, up to effective size N_H at 7 ka. Model 1c is the same, except that there is also a bottleneck during the LGM. In this model the original European population first grows to N_{LGM} at 25 ka, then is reduced to constant proportion P_{LGM} throughout the LGM. After the end of the LGM at 19.5 ka, model 1c is identical to model 1b. In model 2a, a split occurs in the pre-LGM population at time T_S, with the new population having constant size N_S. The original population then goes extinct at the beginning of the LGM, and the new population re-expands following the LGM, up to N_H at 7 ka. Model 2b is similar, except that the pre-LGM population survives through an LGM bottleneck up until the beginning of the Late Glacial, but is then replaced by the new population, expanding at the end of the Late Glacial. Model 3 assumes that both the LGM and the Late Glacial caused population replacements, with each new population diverging from the previous one (at times T_S and T_{S2}) prior to the replacement event. All parameter prior distributions are reported in Table S5.

Model choice procedure

Previous authors have suggested that posterior probabilities of multiple competing models may be estimated in the ABC framework by calculating the proportion of accepted simulations from each model below a certain tolerance δ in a common ranked pool [S61]. However, it has been demonstrated that this approach is not theoretically justified [S62], as the loss of information in reducing the data to summary statistics means that this approximation is not guaranteed to converge on the true Bayes factors. We performed model choice using the multinomial logistic regression approach introduced by Beaumont [S58], which treats a model indicator as a categorical variable and returns an estimate of the posterior probability for each model. In order to evaluate this procedure we nested it in a simulation-based power-analysis similar to that of Veeramah *et al.* [S59], where datasets generated under each of the six models defined above are used as pseudo-observed data. Firstly, for each model we simulated 10^6 datasets and 50 independent datasets to act as pseudo-observed data. Then, given a set of summary statistics S and a tolerance level δ (discussed below), we iterated through each of the 300 pseudo-observed datasets, each time performing the rejection and multinomial logistic regression steps (using the VGAM R package by Yee TW, https://www.stat.auckland.ac.nz/~yee/VGAM), using the highest posterior probability criterion to select the best model. Power was then approximated by the proportion of times this procedure identified the correct model.

The choice of appropriate statistics S in ABC model comparison (and in general) is still a difficult and unresolved problem, so we followed the heuristic approach implemented by Veeramah *et al*. [S59], in which a set of candidate summary statistics are ranked according to their p-value from a Kruskal-Wallis test applied to a random sample of 10,000 simulations from each model. The idea is that a lower p-value suggests a greater difference in the medians of the statistic distributions across models, and hence provides greater power to distinguish between models. In order to minimize bias for or against any particular model,

we group statistics by family, e.g. all within-group mean pairwise differences (π_i) are grouped, and rank these blocks using their median p-value. Global statistics (e.g. global mean pairwise differences π_{all}) are added as blocks individually. We iteratively added new summary statistic blocks from the ranked list (Table S6) to our set *S* in our analysis. Within-group statistics for the 'Pre-LGM' sample group were excluded *a priori* given that they appear in the same position in each model and thus have no significant between-model discriminatory power. The choice of tolerance δ in the ABC rejection algorithm is also difficult to fix objectively so, again following Veeramah *et al.* [S59], we iteratively repeated the analysis accepting between 1000 and 10,000 simulations in steps of 1000. Iterating across the number of summary statistics and the number of retained simulations we found the combination (*S*,δ) with maximal power to discriminate between all competing models.

The combination (*S*,δ) that maximizes the power (0.650) for this model choice procedure is δ = 5000 and *S* comprises the first 10 statistics blocks given in Table S6. Using these values applied to our observed data we find that model 2b has by far the highest posterior probability (0.807). All 6 model posterior probabilities are given in Figure S2.

Parameter estimation

Following the identification of 2b as the best-fitting model, a further four million coalescent simulations were run as previously described, giving five million in total. We performed ABC with local-linear multivariate weighted regression adjustment [S60], assuming a tolerance $F\delta$ = 0.25% so that 12,500 simulations were retained. Other tolerance values of 0.1% and 0.5% gave almost identical results. We used 5 within-group statistics (number of haplotypes, number of segregating sites, mean pairwise difference π, haplotype diversity *H* and Tajima's *D*) for each of the four chronological sample groups described above (see Table S6), and two between-group statistics (mean pairwise difference π and F_{ST}) for each pair, giving a total of 32 summary statistics. Observed values of each summary statistic are given in Table S6, and marginal posterior densities for each parameter are given in Table S5.

Archeological site information

The 35 Upper Paleolithic and Mesolithic human specimens, from which we sequenced complete mtDNA, were obtained from 21 archeological sites across Europe. For each human remains, a portion or the entire specimen was collected from archeological collections in Belgium, Romania, Italy, Czech Republic, France and Germany and sampled in the dedicated ancient DNA laboratory facility of the University of Tübingen, in Germany. All samples were directly or stratigraphically radiocarbon dated. Newly reported ^{14}C dates were calibrated using Reimer et al.'s [S17] calibration curve (Table S1). In the main text and in the Supplemental Experimental Procedures, the date unit reported is thousands of calibrated years before present (ka) unless otherwise specified.

Peştera Cioclovina Uscată (South Transylvania, Romania)

The calvaria Cioclovina1 was discovered in Uscată located in South Transylvania. The specimen was recently radiocarbon dated to 28,510 ± 170 ^{14}C years before present [S4], placing this individual among the oldest human specimens found in Central and South-Eastern Europe. The complete mtDNA genome recovered from a cranial fragment shows a basal phylogenetic position compared to all modern day humans belonging to haplogroup U. This confirms its affinity to modern humans at the mtDNA level as previously reported from geometric morphometric analyses [S63].

La Rochette (Dordogne, France)

Otto Hauser first excavated the Middle and Upper Paleolithic site of La Rochette close to Saint-Léon-sur-Vézère in 1910. He identified human occupations of the site spanning from the Mousterian to the Magdalenian. Human remains were originally assigned to a general Aurignacian layer. However, a revision of the stratigraphy [S64] reconsidered its division into three distinct horizons, i.e. Gravettian, Aurignacian and Chatelperronian. A first ^{14}C AMS dating of a human right ulna was performed in 2002 by Orschiedt and was repeated recently making use of more advanced ultrafiltration techniques [S2]. Both dates consistently fall around 23,000 ^{14}C years before present, associating this human remain to the Gravettian material culture horizon. The dated specimen was also sampled for ancient DNA investigation.

Dolní Věstonice (South Moravia, Czech Republic)
Excavations in the northern slope of the Pavlovské Hills started in 1924 and since then three Gravettian human burial sites have been discovered, namely the Dolní Věstonice I, Dolní Věstonice II and Pavlov I. In the two former sites, human fossils are numbered from DV1 to DV64 and in Pavlov I from 1 to 33. Ancient DNA analysis was performed on individuals DV16 and DV43 both coming from the Dolní Věstonice II site. Radiocarbon dating was performed on earth and charcoal associated to DV16, assigning it to around 30 ka. Both human remains were identified in close vicinity, and were suggested to be of similar age [S5].

Grotta Paglicci (Apulia, Italy)
Grotta Paglicci (Rignano Garganico - Foggia) is located in Apulia, the southeastern-most Italian region. The site comprises the present-day cave and a rock shelter that, in the past, was part of the same cave system and testifies to a human occupation during the Lower-Middle Paleolithic (Acheulean, Early Mousterian). The 12m-thick sequence excavated inside the cave yielded remains extending from the Aurignacian to the Final Epigravettian [S12]. Paglicci is also important for the several human remains uncovered along the Upper Paleolithic sequence and for the most ancient evidence of producing flour [S65]. The investigations were conducted by the Natural History Museum of Verona (F. Zorzi) from 1961 to 1971 and carried out by the University of Siena (first by A. Palma di Cesnola and currently by A. Ronchitelli) in collaboration with the Soprintendenza Archeologia della Puglia.
Radiocarbon dating was performed on archeological layers associated with modern human occupation. The three samples analyzed here belong to three distinct stratigraphic units. Paglicci71 found in layer 8A is associated with the Evolved Epigravettian culture, Paglicci108 in layer 21B with the Evolved Gravettian and Paglicci133 found in layer 23C2, between the Early Gravettian layer 23A and the Aurignacian layer 24A1 [S11, S12, S13]. The volcanic tephra Codola dated elsewhere to around 33 ka [S66] was found in layer 23C2.

Troisième Caverne (Goyet, Belgium)
The Troisième Caverne of Goyet in Belgium was excavated in the latter half of the 19th and beginning of the 20th century, and again at the end of the 1990s. The main excavations were performed in 1868 by Edouard Dupont who identified Paleolithic human occupations [S67] that were later attributed to the Middle and Upper Paleolithic (including Mousterian, Lincombian-Ranisian-Jerzmanowician, Aurignacian, Gravettian and Magdalenian material) as well as to the Neolithic and historic period [S68]. Starting in 2008, the reassessment of both the human and faunal collections from the site yielded new human remains. Due to the lack of detailed documentation of the excavated material, their association to a specific occupation was impossible and a multidisciplinary study of the human remains and their context was undertaken. Morphometric and taphonomic features, completed by the direct radiocarbon dating of the remains, were used to assign them to different periods. In combination with isotopic and genetic analyses [S69, S70] the results allowed for the specimens to be assigned to either late Neanderthals or modern humans. Here we analyzed the mtDNA genomes of two specimens directly dated to the Aurignacian, five to the Gravettian and one to the Magdalenian (Table S1).

Swabian Jura sites (Baden-Württemberg, Germany)
We were able to collect and analyze a total of nine human remains from seven cave sites of the Swabian Jura (Hohle Fels, Brillenhöhle, Burkhardtshöhle, Bockstein-Höhle, Falkensteiner Höhle, Hohlenstein-Stadel and Felsdach Inzigkofen). Those are located in Southwest Germany mainly along the Ach and Lone valleys formed by the homonymous Danube's tributaries. The entire region is composed of Jurassic limestone where karst landscapes lead to cave formations.

- Hohle Fels (Ach valley) is the worldwide famous Swabian Jura site for the discovery of an ivory 'Venus' figurine and bird bone and ivory flutes. These are both dated to the early Aurignacian period and are among the first figurative art and musical instruments ever found in Europe [S71, S72]. In the cave, five human remains have been discovered. Three of them were genetically analyzed in the present study. A left and a right femur fragments were found in close proximity in the Magdalenian stratigraphic layer and may belong to the same individual [S7]. Both were previously genetically characterized as belonging to haplogroup U, based on a short mtDNA amplicon [S6]. In the present study, we reconstructed complete mtDNA genomes for both specimens and a well-supported phylogenetic placement was assigned. The two specimens were found to have an identical haplogroup U8a (with private mutations C150T, G1422A, C16519T) supporting that, if not the same individual, they have a close maternal relationship. A skull

fragment was also identified bearing the same haplotype. Although it was initially assigned to the Gravettian layer [S73], we report here a direct radiocarbon date of the specimen to around 15 ka placing it also within the Magdalenian archeological horizon.

- Brillenhöhle (Ach Valley) was discovered in 1956 and excavated by Gustav Riek. A minimum number of four individuals have been assigned to the Magdalenian techno-complex. The parietal bone fragment genetically analyzed in the present work was directly dated to around 15 ka [S2]. This date is within the typical temporal range of the Magdalenian in the Swabian Jura [S7].
- Burkhardtshöhle (Westerheim, Württemberg) was first excavated in 1933-34 by Gustav Riek, who resumed the excavation in 1953 after the end of World War II. A total of five cranial fragments probably belonging to a single individual were discovered and radiocarbon dating confirmed their assignment to their Magdalenian timeframe [S3].
- Bockstein-Höhle (Lone valley) was discovered in 1883 and first excavated by Bürger. A double burial was identified with an almost complete female skeleton and an infant skeleton at the right end of the female's feet. The infant has been considered as the child of the female individual. Two anatomical elements of the infant were previously radiocarbon dated providing a consistent burial age of around 8 ka and associating it to the Late Mesolithic time period [S1]. The upper right second incisor tooth from the female was sampled and genetically analyzed.
- Falkensteiner Höhle is located close to the village of Bad Urach, southwest from the aforementioned Ach and Lone valleys. Around 40 human skeletal elements were identified during the excavation in 1933 and the analysis of the retrieved material was carried out in 1964 [S7]. As a result, the layer that yielded the human remains with associated microlithic stone tools has been radiocarbon dated to the Early Mesolithic [S74]. The same anatomical element investigated here was genetically analyzed in Bramanti et al. [S6]. Besides confirming the assignment to mtDNA hg U5b2, we were able to reconstruct its complete mtDNA and further define it as haplogroup U5b2a with additional private mutations (A4732G, G8572A, A16171G, C16519T).
- Hohlenstein-Stadel (Lone valley) contains evidence of hominid occupations during the Middle Paleolithic, Upper Paleolithic, Mesolithic and Neolithic. A burial formed by the skulls and cervical vertebras of three individuals (one male, one female and one infant) was discovered and dated to the Late Mesolithic [S9]. Here, we sampled one cervical vertebra for ancient DNA analysis.

Felsdach Inzigkofen (Upper Danube valley, Germany)

The site was discovered in 1965 close to the village of Beuron in the Upper Danube valley and excavated by Wolfgang Taute. A single wisdom tooth analyzed here was discovered in a layer dated to the initial Late Mesolithic phase also known as the Early Atlantic [S7, S74].

Große Ofnet Höhle (Franconian Jura, Germany)

The molar analyzed by ancient DNA belongs to an individual that was found in the Große Ofnet cave close to Nördlingen. It may belong to a burial site formed by 34 skulls of both sexes and different developmental ages, found in two burial pits [S9]. Lithic artifacts and faunal remains (deer canines, snail shells) were found in association with the human remains. All crania were facing west and presented cut-marks [S75]. Several skulls display traumatic injuries, suggesting interpersonal violence. All radiocarbon-dated individuals provided a consistent age around 8 ka and were assigned to the Late Mesolithic [S9].

French Jura sites (Franche-Comté, France)

Three analyzed human specimens were identified in three different prehistoric sites of the French Jura, located along the border between Eastern France and Western Switzerland. This medium size mountainous region is composed of Mesozoic limestone defining a karst landscape [S76].

- Cabônes rockshelter (Ranchot, Jura department) was excavated between 1978 and 1990 and yielded at least five Mesolithic human individuals [S77]. The one genetically analyzed is defined by a reconstructed right parietal bone dated to around 10 ka and assigned to the Middle Mesolithic period.
- Rigney 1 cave (Doubs department) was excavated at the beginning of the 1950s and a human mandible fragment was discovered during a rescue excavation that occurred in 1986 and 1987 at this Magdalenian site [S76]. This bone has been directly radiocarbon dated to around 15.5 ka [S14] and it was sampled for paleogenetic investigation.

• Rochedane rockshelter (Villars-sous-Dampjoux, Doubs department) was discovered at the end of the 19th century and was excavated by A. Thévenin between 1968 and 1976. This site is one of the most important prehistoric Late Glacial sequences in Eastern France [S14]. Several human bones have been found in the Mesolithic and the Final Paleolithic levels. The one genetically analyzed is a mandible dated to around 13 ka and assigned to the Epipaleolithic period.

Paris Basin (France)

The Paris Basin is a geological region in Northeast France formed by sedimentary rocks. The area is characterized by plateau plains where several Mesolithic human burials have been identified [S78].

• Les Closeaux at Rueil-Malmaison is a Mesolithic site located along the river Seine. In sector 3, a circular burial with a single and almost complete human skeleton was found. The individual was buried in a sitting position and has been directly radiocarbon dated to 9.9 ka [S10].

• Les Vignolles at Mareuil-lès-Meaux is an archeological site on the river Marne. The oldest inhumation that was discovered at the site is a single burial directly dated to the Mesolithic time [S10]. However, the presence of additional Neolithic burials and a Bronze Age necropolis attested to occupations of the site also during later periods [S79].

• Les Fontinettes at Cuiry-lès-Chaudardes is a multi-period site with an important early Neolithic (LBK) settlement. The Mesolithic burial was found on the edge of the site. The individual, in a squatting position, had a necklace of fish vertebrae and the burial contained three flint bladeless [S80]. The skeleton has been dated to around 8 ka.

• Le Vieux Tordoir at Berry-au-Bac is also a multi-period site, including an early Neolithic (LBK) settlement. One Mesolithic burial was discovered on the site. The deceased was buried in a seated position with ochre and a bone tool [S81]. The skeleton has been dated to around 7 ka.

Aven des Iboussières à Malataverne (Rhône-Alpes, France)

The site is located in the Drôme department of South France. A minimum number of eight human individuals were found at the Aven des Iboussières and were interpreted as burials of Epipaleolithic hunter-gatherers [S82]. We obtained complete mtDNA genomes from three individuals: Iboussieres25-1, Iboussieres31-2 and Iboussieres39. Only the latter, a left femur fragment, was directly radiocarbon dated to 11.8 ka. Nonetheless, the date overlaps with that of a faunal remain from the site (10210 ± 80 uncal BP; OxA5682) [S83], suggesting that all burials belong to the same temporal unit.

Climatic considerations and time definitions

The oldest possible evidence of early modern humans in Europe, found in Southern Italy, dates back to ~45 ka [S2]. Europeans relied uniquely on a foraging lifestyle for almost 40,000 years, from the first arrival to the spread of farming (~8 ka). This time spans the end of the Late Pleistocene (130 – 11.5 ka) and the beginning of the Holocene epochs (11.5ka – today) and represents around three-quarters of the time during which modern humans occupied Europe. This period (45 – 8 ka) was affected by severe climatic fluctuations and repeated environmental changes [S84]. Such phenomena are captured by the extended INTIMATE oxygen-18 oscillation curve [S85] (Figure 3) recorded by the North Greenland Ice-Core Project (NGRIP) [S86]. The observed values along this timeline correlate indirectly with the temperatures of the Northern Hemisphere and separate time into Marine Isotope Stages (MIS). Those represent relatively consistent warm interglacial (odd numbers) or cold glacial (even numbers) intervals alternating through time and numbered going back in time from the present day interglacial MIS1.

The time interval investigated in this study (45 – 7 ka) span across three climatically distinct periods: MIS3, MIS2 and MIS1 (from the past to the present). During the general warm MIS3 (~57 – 29 ka), there were dramatic fluctuations of climatic conditions spanning ~1,000 years intervals [S87]. It has been suggested that the spread of modern humans from the Near East into Europe was favored by a climatic warming phase during the MIS3 [S88]. Figure 1A depicts one of these relatively warm phase around 39 – 36 ka with sea level about 60 meters below present level [S84]. The mitigated climatic conditions reduced the ice sheet diffusion with a retraction of the steppe-tundra landscape towards Northern Europe [S84]. However environmental conditions kept on changing for the next millennia during an attested human occupation of Europe (Pre-LGM in Figure 3).

With the start of MIS2 (~29 ka), a general trend of temperature reduction began until the onset of the Last Glacial Maximum (LGM) ~25ka when all ice sheets reached their maximal extension since the last glacial

period and the sea level was approximately 130m lower than today [S89, S90] During this period, that lasted until ~19.5 ka, ice caps covered most of Northern Europe, the Alps and the Pyrenees mountain chains [S91, S92]. These cold and dry conditions throughout Europe prevented human occupation of North-Western Europe and likely forced migrations to climatic and environmental refugia [S90]. Proposed areas for human refugia during the LGM are the Mediterranean regions of Franco-Cantabria and Southern Italy, the Balkans and the East European Plain [S93]. Those geographical areas were less impacted by harsh climatic conditions and would have allowed human survival [S94].

With the end of the LGM, humans spread again into central Europe during a period we designated as the post-LGM (Figure 1B, ~19.5 – 14.5 ka), following a general retraction of the Alpine and Pyrenean ice caps and a fragmentation of the North European ice sheet into the Scandinavian and the British ice sheets [S95]. Sea levels were around 100m lower than currently [S96], exposing a vast area of land, known as Doggerland, which is now covered by the Southern North Sea. The bridge of land that connected Great Britain to main Europe lasted until ~8.5ka, when it was covered by the rising sea levels [S97].

The glacial MIS2 phase terminates with the end of the Pleistocene. This period we refer to as the Late Glacial (Figure 1C) is characterized by abrupt climatic variations starting with the warm Bølling/Allerød interstadial (14.5 – 12.7 ka) and ending with the cold Younger Dryas stadial (12.7 – 11.5ka) [S98]. During the first phase, temperatures rose dramatically over the MIS2 average, causing a radical change in European flora that triggered the spread of natural forestation towards Northern Europe [S99]. Those warmer climatic stages are also likely connected with the large extinction of Pleistocene megafauna species and a general turnover in mammalian diversity [S100, S101]. In the following Younger Dryas, the final stage of the last glacial, European average temperature sharply decreased within a few years [S102]. The impact of climatic and environmental fluctuations on human populations at the end of the Pleistocene is largely unknown. However, climate might have played a role in the mtDNA composition shift observed in this study with the beginning of the Late Glacial.

The Holocene starts around 11.5 ka within the MIS1 phase that is characterized by a warm and moist climate, which continues until today. Temperatures rose simultaneously with the sea level and by 7 ka almost all coastlines were in a similar location as nowadays (Figure 1D) [S97]. Holocene hunter-gatherers persisted with a distinct genetic signature at least until ~5 ka in Northern Europe [S18]. The Neolithic transition reached central Europe ~8 ka with the arrival of agricultural communities that drastically changed the existing European genetic makeup [S25].

Supplemental references:

S1. Wehrberger, K. (2000). „Der Streit ward definitiv beendet...” Eine mesolithische Bestattung aus der Bocksteinhöhle im Lonetal, Alb-Donau-Kreis. Zur Erinnerung an Ludwig Bürger (1844-1898). Archäologisches Korrespondenzblatt *30*, 15-31.

S2. Benazzi, S., Douka, K., Fornai, C., Bauer, C.C., Kullmer, O., Svoboda, J., Pap, I., Mallegni, F., Bayle, P., Coquerelle, M., et al. (2011). Early dispersal of modern humans in Europe and implications for Neanderthal behaviour. Nature *479*, 525-528.

S3. Simon, U. (1993). Die Burkhardtshöhle - eine Magdalénienstation am Nordrand der Schwäbischen Alb. (Eberhard-Karls-Universität Tübingen: Magisterarbeit).

S4. Soficaru, A., Petrea, C., Dobos, A., and Trinkaus, E. (2007). The human cranium from the Pestera Cioclovina Uscata, Romania - Context, age, taphonorny, morphology, and paleopathology. Curr Anthropol *48*, 611-619.

S5. Trinkaus, E., and Svoboda, J. (2006). Early Modern Human Evolution in Central Europe: The People of Dolní Věstonice and Pavlov, Volume 12, (Oxford University Press).

S6. Bramanti, B., Thomas, M.G., Haak, W., Unterlaender, M., Jores, P., Tambets, K., Antanaitis-Jacobs, I., Haidle, M.N., Jankauskas, R., Kind, C.J., et al. (2009). Genetic discontinuity between local hunter-gatherers and central Europe's first farmers. Science *326*, 137-140.

S7. Haas-Campen, S. (1993). Die menschlichen Skelettreste des Spätpleistozäns und Frühholozäns in Baden-Württemberg. In Geowissenschaftliche Fakultät, Institut für Humangenetik und Anthropologie. (Eberhard-Karls-Universität Tübingen: Magisterarbeit).

S8. Housley, R.A., Gamble, C.S., Street, M., and Pettitt, P.B. (1997). Radiocarbon evidence for the Lateglacial human recolonisation of Norther Europe. Proc. Prehist. Soc. *63*, 25-54.

S9. Orschiedt, J. (1999). Manipulationen an menschlichen Skelettresten. Taphonomische Prozesse, Sekundärbestattungen oder Kannibalismus. Dissertation. Urgeschichtliche Materialhefte *13*.

S10. Valentin, F., COTTIAUX R., C., B.-M., CONFALONIERI J., DELATTRE V., LANG L., LE GOFF I., LAWRENCE-DUBOVAC P., and C., V. (2008). Découvertes récentes d‘inhumations et d’incinération datées du Mésolithique en Ile de France. Revue Archéologique d’Ile-de-France, 21-42.

S11. Azzi, C.M., Bigliocca , L., and Piovan, F. (1974). Florence Radiocarbon Dates II. Radiocarbon *16*, 10-14.

S12. Palma di Cesnola, A. (2004). Paglicci. L’Aurignaziano e il Gravettiano antico, (Foggia: Claudio Grenzi Ed.).

S13. Azzi, C.M., Bigliocca , L., and Piovan, F. (1977). Florence Radiocarbon Dates III. Radiocarbon *19*, 165-169.

S14. Cupillard, C., Magny, M., Bocherens, H., Bridault, A., Begeot, C., Bichet, V., Bossuet, G., Drucker, D.G., Gauthier, E., Jouannic, G., et al. (2015). Changes in ecosystems, climate and societies in the Jura Mountains between 40 and 8 ka cal BP. Quaternary International *378*, 40-72.

S15. Renaud, G., Slon, V., Duggan, A.T., and Kelso, J. (2015). Schmutzi: estimation of contamination and endogenous mitochondrial consensus calling for ancient DNA. Genome Biol *16*, 224.

S16. Drummond, A.J., and Rambaut, A. (2007). BEAST: Bayesian evolutionary analysis by sampling trees. BMC Evol Biol *7*, 214.

S17. Reimer, P.J., Bard, E., Bayliss, A., Beck, J.W., Blackwell, P.G., Ramsey, C.B., Buck, C.E., Cheng, H., Edwards, R.L., Friedrich, M., et al. (2013). Intcal13 and Marine13 Radiocarbon Age Calibration Curves 0-50,000 Years Cal Bp. Radiocarbon *55*, 1869-1887.

S18. Skoglund, P., Malmstrom, H., Omrak, A., Raghavan, M., Valdiosera, C., Gunther, T., Hall, P., Tambets, K., Parik, J., Sjogren, K.G., et al. (2014). Genomic diversity and admixture differs for Stone-Age Scandinavian foragers and farmers. Science *344*, 747-750.

S19. Bollongino, R., Nehlich, O., Richards, M.P., Orschiedt, J., Thomas, M.G., Sell, C., Fajkosova, Z., Powell, A., and Burger, J. (2013). 2000 years of parallel societies in Stone Age Central Europe. Science *342*, 479-481.

S20. Fu, Q., Mittnik, A., Johnson, P.L., Bos, K., Lari, M., Bollongino, R., Sun, C., Giemsch, L., Schmitz, R., Burger, J., et al. (2013). A revised timescale for human evolution based on ancient mitochondrial genomes. Curr Biol *23*, 553-559.

S21. Sanchez-Quinto, F., Schroeder, H., Ramirez, O., Avila-Arcos, M.C., Pybus, M., Olalde, I., Velazquez, A.M., Marcos, M.E., Encinas, J.M., Bertranpetit, J., et al. (2012). Genomic affinities of two 7,000-year-old Iberian hunter-gatherers. Curr Biol *22*, 1494-1499.
S22. Benazzi, S., Slon, V., Talamo, S., Negrino, F., Peresani, M., Bailey, S.E., Sawyer, S., Panetta, D., Vicino, G., Starnini, E., et al. (2015). Archaeology. The makers of the Protoaurignacian and implications for Neandertal extinction. Science *348*, 793-796.
S23. Ermini, L., Olivieri, C., Rizzi, E., Corti, G., Bonnal, R., Soares, P., Luciani, S., Marota, I., De Bellis, G., Richards, M.B., et al. (2008). Complete mitochondrial genome sequence of the Tyrolean Iceman. Curr Biol *18*, 1687-1693.
S24. Krause, J., Briggs, A.W., Kircher, M., Maricic, T., Zwyns, N., Derevianko, A., and Paabo, S. (2010). A complete mtDNA genome of an early modern human from Kostenki, Russia. Curr Biol *20*, 231-236.
S25. Lazaridis, I., Patterson, N., Mittnik, A., Renaud, G., Mallick, S., Kirsanow, K., Sudmant, P.H., Schraiber, J.G., Castellano, S., Lipson, M., et al. (2014). Ancient human genomes suggest three ancestral populations for present-day Europeans. Nature *513*, 409-413.
S26. Raghavan, M., Skoglund, P., Graf, K.E., Metspalu, M., Albrechtsen, A., Moltke, I., Rasmussen, S., Stafford, T.W., Jr., Orlando, L., Metspalu, E., et al. (2014). Upper Palaeolithic Siberian genome reveals dual ancestry of Native Americans. Nature *505*, 87-91.
S27. Fu, Q., Hajdinjak, M., Moldovan, O.T., Constantin, S., Mallick, S., Skoglund, P., Patterson, N., Rohland, N., Lazaridis, I., Nickel, B., et al. (2015). An early modern human from Romania with a recent Neanderthal ancestor. Nature *524*, 216-219.
S28. Gilbert, M.T., Kivisild, T., Gronnow, B., Andersen, P.K., Metspalu, E., Reidla, M., Tamm, E., Axelsson, E., Gotherstrom, A., Campos, P.F., et al. (2008). Paleo-Eskimo mtDNA genome reveals matrilineal discontinuity in Greenland. Science *320*, 1787-1789.
S29. Fu, Q., Li, H., Moorjani, P., Jay, F., Slepchenko, S.M., Bondarev, A.A., Johnson, P.L., Aximu-Petri, A., Prufer, K., de Filippo, C., et al. (2014). Genome sequence of a 45,000-year-old modern human from western Siberia. Nature *514*, 445-449.
S30. Jones, E.R., Gonzalez-Fortes, G., Connell, S., Siska, V., Eriksson, A., Martiniano, R., McLaughlin, R.L., Gallego Llorente, M., Cassidy, L.M., Gamba, C., et al. (2015). Upper Palaeolithic genomes reveal deep roots of modern Eurasians. Nat Commun *6*, 8912.
S31. Dabney, J., Knapp, M., Glocke, I., Gansauge, M.T., Weihmann, A., Nickel, B., Valdiosera, C., Garcia, N., Paabo, S., Arsuaga, J.L., et al. (2013). Complete mitochondrial genome sequence of a Middle Pleistocene cave bear reconstructed from ultrashort DNA fragments. Proc Natl Acad Sci U S A *110*, 15758-15763.
S32. Rohland, N., and Hofreiter, M. (2007). Ancient DNA extraction from bones and teeth. Nat Protoc *2*, 1756-1762.
S33. Meyer, M., and Kircher, M. (2010). Illumina sequencing library preparation for highly multiplexed target capture and sequencing. Cold Spring Harb Protoc *2010*, pdb prot5448.
S34. Kircher, M., Sawyer, S., and Meyer, M. (2012). Double indexing overcomes inaccuracies in multiplex sequencing on the Illumina platform. Nucleic Acids Res *40*, e3.
S35. Schuenemann, V.J., Singh, P., Mendum, T.A., Krause-Kyora, B., Jager, G., Bos, K.I., Herbig, A., Economou, C., Benjak, A., Busso, P., et al. (2013). Genome-wide comparison of medieval and modern Mycobacterium leprae. Science *341*, 179-183.
S36. Ruano, G., and Kidd, K.K. (1992). Modeling of heteroduplex formation during PCR from mixtures of DNA templates. PCR Methods Appl *2*, 112-116.
S37. Maricic, T., Whitten, M., and Paabo, S. (2010). Multiplexed DNA sequence capture of mitochondrial genomes using PCR products. PLoS One *5*, e14004.
S38. Kao, W.C., Stevens, K., and Song, Y.S. (2009). BayesCall: A model-based base-calling algorithm for high-throughput short-read sequencing. Genome Res *19*, 1884-1895.
S39. Kircher, M. (2012). Analysis of high-throughput ancient DNA sequencing data. Methods Mol Biol *840*, 197-228.
S40. Li, H., and Durbin, R. (2009). Fast and accurate short read alignment with Burrows-Wheeler transform. Bioinformatics *25*, 1754-1760.
S41. Peltzer, A., Jäger, G., Herbig, A., Seitz, A., Kniep, C., Krause, J., and Nieselt, K. (subm.). EAGER: Efficient Ancient Genome Reconstruction. Genome Res.

S42. Li, H., Handsaker, B., Wysoker, A., Fennell, T., Ruan, J., Homer, N., Marth, G., Abecasis, G., Durbin, R., and Genome Project Data Processing, S. (2009). The Sequence Alignment/Map format and SAMtools. Bioinformatics *25*, 2078-2079.
S43. van Oven, M., and Kayser, M. (2009). Updated comprehensive phylogenetic tree of global human mitochondrial DNA variation. Hum Mutat *30*, E386-394.
S44. Kloss-Brandstatter, A., Pacher, D., Schonherr, S., Weissensteiner, H., Binna, R., Specht, G., and Kronenberg, F. (2011). HaploGrep: a fast and reliable algorithm for automatic classification of mitochondrial DNA haplogroups. Hum Mutat *32*, 25-32.
S45. Behar, D.M., van Oven, M., Rosset, S., Metspalu, M., Loogvali, E.L., Silva, N.M., Kivisild, T., Torroni, A., and Villems, R. (2012). A "Copernican" reassessment of the human mitochondrial DNA tree from its root. Am J Hum Genet *90*, 675-684.
S46. Kearse, M., Moir, R., Wilson, A., Stones-Havas, S., Cheung, M., Sturrock, S., Buxton, S., Cooper, A., Markowitz, S., Duran, C., et al. (2012). Geneious Basic: an integrated and extendable desktop software platform for the organization and analysis of sequence data. Bioinformatics *28*, 1647-1649.
S47. Edgar, R.C. (2004). MUSCLE: multiple sequence alignment with high accuracy and high throughput. Nucleic Acids Res *32*, 1792-1797.
S48. Ingman, M., Kaessmann, H., Paabo, S., and Gyllensten, U. (2000). Mitochondrial genome variation and the origin of modern humans. Nature *408*, 708-713.
S49. Tamura, K., Stecher, G., Peterson, D., Filipski, A., and Kumar, S. (2013). MEGA6: Molecular Evolutionary Genetics Analysis version 6.0. Mol Biol Evol *30*, 2725-2729.
S50. Keane, T.M., Creevey, C.J., Pentony, M.M., Naughton, T.J., and McLnerney, J.O. (2006). Assessment of methods for amino acid matrix selection and their use on empirical data shows that ad hoc assumptions for choice of matrix are not justified. BMC Evol Biol *6*, 29.
S51. Huelsenbeck, J.P., and Ronquist, F. (2001). MRBAYES: Bayesian inference of phylogenetic trees. Bioinformatics *17*, 754-755.
S52. Rieux, A., Eriksson, A., Li, M., Sobkowiak, B., Weinert, L.A., Warmuth, V., Ruiz-Linares, A., Manica, A., and Balloux, F. (2014). Improved calibration of the human mitochondrial clock using ancient genomes. Mol Biol Evol *31*, 2780-2792.
S53. Ferreira, M.A.R., and Suchard, M.A. (2008). Bayesian analysis of elapsed times in continuous-time Markov chains. Can J Stat *36*, 355-368.
S54. Baele, G., Lemey, P., and Vansteelandt, S. (2013). Make the most of your samples: Bayes factor estimators for high-dimensional models of sequence evolution. BMC Bioinformatics *14*, 85.
S55. Mellars, P., Gori, K.C., Carr, M., Soares, P.A., and Richards, M.B. (2013). Genetic and archaeological perspectives on the initial modern human colonization of southern Asia. Proc Natl Acad Sci U S A *110*, 10699-10704.
S56. Anderson, C.N., Ramakrishnan, U., Chan, Y.L., and Hadly, E.A. (2005). Serial SimCoal: a population genetics model for data from multiple populations and points in time. Bioinformatics *21*, 1733-1734.
S57. Bandelt, H.J., Salas, A., and Bravi, C.M. (2006). What is a 'novel' mtDNA mutation--and does 'novelty' really matter? J Hum Genet *51*, 1073-1082.
S58. Beaumont, M. (2008). Joint determination of topology, divergence time and immigration in population trees. In Simulations, genetics and human prehistory, S. Matsumura, P. Forster and C. Renfrew, eds. (Cambridge: McDonald Institute for Archaeological Research), pp. 135-154.
S59. Veeramah, K.R., Wegmann, D., Woerner, A., Mendez, F.L., Watkins, J.C., Destro-Bisol, G., Soodyall, H., Louie, L., and Hammer, M.F. (2012). An early divergence of KhoeSan ancestors from those of other modern humans is supported by an ABC-based analysis of autosomal resequencing data. Mol Biol Evol *29*, 617-630.
S60. Beaumont, M.A., Zhang, W., and Balding, D.J. (2002). Approximate Bayesian computation in population genetics. Genetics *162*, 2025-2035.
S61. Pritchard, J.K., Seielstad, M.T., Perez-Lezaun, A., and Feldman, M.W. (1999). Population growth of human Y chromosomes: a study of Y chromosome microsatellites. Mol Biol Evol *16*, 1791-1798.
S62. Robert, C.P., Cornuet, J.M., Marin, J.M., and Pillai, N.S. (2011). Lack of confidence in approximate Bayesian computation model choice. Proc Natl Acad Sci U S A *108*, 15112-15117.

S63. Harvati, K., Gunz, P., and Grigorescu, D. (2007). Cioclovina (Romania): affinities of an early modern European. J Hum Evol *53*, 732-746.
S64. Delporte, H. (1962). Le gisement paléolithique de la Rochette, commune de Saint-Léon-sur-Vézère, Dordogne. Gallia Préhistoire *V*, 1-22.
S65. Lippi, M.M., Foggi, B., Aranguren, B., Ronchitelli, A., and Revedin, A. (2015). Multistep food plant processing at Grotta Paglicci (Southern Italy) around 32,600 cal BP. P Natl Acad Sci USA *112*, 12075-12080.
S66. Giaccio, B., Isaia, R., Fedele, F.G., Di Canzio, E., Hoffecker, J., Ronchitelli, A., Sinitsyn, A.A., Anikovich, M., Lisitsyn, S.N., and Popov, V.V. (2008). The Campanian Ignimbrite and Codola tephra layers: Two temporal/stratigraphic markers for the Early Upper Palaeolithic in southern Italy and eastern Europe. J Volcanol Geoth Res *177*, 208-226.
S67. Dupont, E. (1872). L'Homme pendant les âges de la pierre dans les environs de Dinant-sur-Meuse, Volume 2ème édition, (Bruxelles: C. Muquardt Ed.).
S68. Flas, D. (2006). La transition du Paléolithique moyen au supérieur dans la plaine septentrionale de l'Europe. Les problématiques du Lincombien-Ranisien-Jerzmanowicien. Volume 119. (Université de Liège: PhD dissertation), p. 254.
S69. Wißing, C., Rougier, H., Crevecoeur, I., Germonpré, M., Naito, Y.I., Semal, P., and Bocherens, H. (in press). Isotopic evidence for dietary ecology of Late Neandertals in North-Western Europe. Quat Int.
S70. Rougier, H., Crevecoeur, I., Beauval, C., Posth, C., Flas, D., Wißing, C., Furtwängler, A., Germonpré, M., Gómez-Olivencia, A., Semal, P., et al. (subm.). Neandertal cannibalism at the Troisième caverne of Goyet (Belgium).
S71. Conard, N.J., Malina, M., and Munzel, S.C. (2009). New flutes document the earliest musical tradition in southwestern Germany. Nature *460*, 737-740.
S72. Conard, N.J. (2009). A female figurine from the basal Aurignacian of Hohle Fels Cave in southwestern Germany. Nature *459*, 248-252.
S73. Conard, N.J., and Bolus, M. (2003). Radiocarbon dating the appearance of modern humans and timing of cultural innovations in Europe: new results and new challenges. J Hum Evol *44*, 331-371.
S74. Holdermann, C.-S., and Kind, C.-J. (2009). Zeitwechsel in Schichten. Bedeutende Fundstellen an der oberen Donau. Eiszeit. Kunst und Kultur. Begleitband zur Großen Landesausstellung Eiszeit - Kunst und Kultur im Kunstgebäude Stuttgart, 332–335.
S75. Mollison, T. (1936). Zeichen gewaltsamer Verletzungen an den Ofnet-Schädeln. Anthrop. An. *13*, 79-88.
S76. Cupillard, C., Malgarini, R., and Fornage-Bontemps, S. (2013). Le Paléolithique supérieur ancien dan le quart nord-est de la France : l'exemple de la Franche-Comté. Environnement, chronologie et faciès culturels. Mémoire LVI de la Société préhistorique française, 351 – 363.
S77. Valentin, F. (1998). Les restes humains de l'abri des Cabônes à Ranchot (Jura). In : Les derniers chasseurs-cueilleurs (13000-5500 av. JC) dans le massif du Jura et ses marges. Centre Jurassien du Patrimoine, 185-186.
S78. Bosset, G., and Valentin, F. (2013). Mesolithic burial practices in the northern half of France: Isolated burials and their spatial organisation. Paris: Société préhistorique française, 207-216.
S79. Cottiaux, R., Delattre, V., Lawrence-Dunovac, P., and Durand, S. (2001). Les occupations néolitiques et protohistoriques du site Mareuil-lès-Meaux "les Vignolles" (Seine-et-Marne), résultats préliminares. Achtes des Journées Archéologiques d' Île-de-France, 60-63.
S80. Ilett, M. (1998). Cuiry-lès-Chaudardes "les Fontinettes". In Rapport de fouille programmée. (Université de Paris 1-Panthéon Sorbonne: Ministère de la Culture).
S81. Auxiette, G., and Hachem, L. (1989). Berry-au-Bac, "Le Chemin de la Pêcherie ouest", "le Vieux-Tordoir", "la culée". (Fouille Protohistorique de la Vallée de l'Aisne: Ministère de la Culture).
S82. Gely, B., and Morand, P. (1998). Les sépultures épipaléolithiques de l'aven des Iboussières à Malataverne (Drôme, France): Premiers résultats. Ardèche Archéologie *15*, 13-18.
S83. Chaix, L. (2005). Hétéroclite et éclectique: la faune épipaléolithique de l'Aven des Iboussières (Drôme, France). Antropologia-Arkeologia *57*, 411-420.
S84. Van Andel, T.H., and Tzedakis, P.C. (1996). Palaeolothic landscapes of Europe and environs, 150,00-25,000 years ago: an overview. Quaternary Science Reviews *15*, 481-500.

S85. Blockley, S.P.E., Lane, C.S., Hardiman, M., Rasmussen, S.O., Seierstad, I.K., Steffensen, J.P., Svensson, A., Lotter, A.F., Turney, C.S.M., and Bronk Ramsey, C. (2012). Synchronisation of palaeoenvironmental records over the last 60,000 years, and an extended INTIMATE event stratigraphy to 48,000 b2k. Quaternary Science Reviews *36*, 2-10.

S86. Andersen, K.K., Azuma, N., Barnola, J.M., Bigler, M., Biscaye, P., Caillon, N., Chappellaz, J., Clausen, H.B., Dahl-Jensen, D., Fischer, H., et al. (2004). High-resolution record of Northern Hemisphere climate extending into the last interglacial period. Nature *431*, 147-151.

S87. Huijzer, A.S., and Isarin, R.F.B. (1997). The reconstruction of past climates using multi-proxy evidence: an example of the Weichselian Pleniglacial in northwest and central Europe. Quaternary Science Reviews *16*, 513-533.

S88. Macaulay, V., Hill, C., Achilli, A., Rengo, C., Clarke, D., Meehan, W., Blackburn, J., Semino, O., Scozzari, R., Cruciani, F., et al. (2005). Single, rapid coastal settlement of Asia revealed by analysis of complete mitochondrial genomes. Science *308*, 1034-1036.

S89. Clark, P.U., Dyke, A.S., Shakun, J.D., Carlson, A.E., Clark, J., Wohlfarth, B., Mitrovica, J.X., Hostetler, S.W., and McCabe, A.M. (2009). The Last Glacial Maximum. Science *325*, 710-714.

S90. Gamble, C., Davies, W., Pettitt, P., and Richards, M. (2004). Climate change and evolving human diversity in Europe during the last glacial. Philos Trans R Soc Lond B Biol Sci *359*, 243-253; discussion 253-244.

S91. Carr, S.J., Holmes, R., Van der Meer, J.J.M., and Rose, J. (2006). The Last Glacial Maximum in the North Sea Basin: micromorphological evidence of extensive glaciation. J Quaternary Sci *21*, 131-153.

S92. Ivy-Ochs, S., Kerschner, H., Kubik, P.W., and Schluchter, C. (2006). Glacier response in the European Alps to Heinrich Event 1 cooling: the Gschnitz stadial. J Quaternary Sci *21*, 115-130.

S93. Soares, P., Achilli, A., Semino, O., Davies, W., Macaulay, V., Bandelt, H.J., Torroni, A., and Richards, M.B. (2010). The archaeogenetics of Europe. Curr Biol *20*, R174-183.

S94. Gamble, C., Davies, W., Pettitt, P., Hazelwood, L., and Richards, M. (2005). The Archaeological and Genetic Foundations of the European Population during the Late Glacial: Implications for. Cambridge Archaeological Journal *15*, 193.

S95. Clark, C.D., Evans, D.J.A., Khatwa, A., Bradwell, T., Jordan, C.J., Marsh, S.H., Mitchell, W.A., and Bateman, M.D. (2004). Map and GIS database of glacial landforms and features related to the last British Ice Sheet. Boreas *33*, 359-375.

S96. Weaver, A.J., Saenko, O.A., Clark, P.U., and Mitrovica, J.X. (2003). Meltwater pulse 1A from Antarctica as a trigger of the bolling-allerod warm interval. Science *299*, 1709-1713.

S97. Gaffney, V.L., Thomson, K., and Fitch, S. (2007). Mapping Doggerland: the Mesolithic landscapes of the southern North Sea, (Oxford: Archaeopress).

S98. Heiri, O., Brooks, S.J., Renssen, H., Bedford, A., Hazekamp, M., Ilyashuk, B., Jeffers, E.S., Lang, B., Kirilova, E., Kuiper, S., et al. (2014). Validation of climate model-inferred regional temperature change for late-glacial Europe. Nat Commun *5*, 4914.

S99. Stewart, J.R., and Lister, A.M. (2001). Cryptic northern refugia and the origins of the modern biota. Trends Ecol Evol *16*, 608-613.

S100. Stuart, A.J., and Lister, A.M. (2012). Extinction chronology of the woolly rhinoceros Coelodonta antiquitatis in the context of late Quaternary megafaunal extinctions in northern Eurasia. Quaternary Science Reviews *51*, 1-17.

S101. Cooper, A., Turney, C., Hughen, K.A., Brook, B.W., McDonald, H.G., and Bradshaw, C.J. (2015). PALEOECOLOGY. Abrupt warming events drove Late Pleistocene Holarctic megafaunal turnover. Science *349*, 602-606.

S102. Severinghaus, J.P., and Brook, E.J. (1999). Abrupt climate change at the end of the last glacial period inferred from trapped air in polar Ice. Science *286*, 930-934.